國 立 交 通 大 學

應用化學系碩士班
碩 士 論 文

核鹼基模型化合物 4(3*H*)-嘧啶酮於溶液相的電場調變

紅外線吸收光譜學

Infrared electroabsorption spectroscopic study of a nucleobase model compound 4(3*H*)-pyrimidinone in solution

研究生: 胡書瑋

指導教授:重藤真介 博士

中華民國 一百零二 年 七 月

核鹼基模型化合物 4(3*H*)-嘧啶酮於溶液相的電場調變紅外線吸收光譜學

Infrared electroabsorption spectroscopic study of a nucleobase model compound 4(3*H*)-pyrimidinone in solution

研究生：胡書瑋　　Student: Shu-Wei Hu

指導教授：重藤真介 博士　　Advisor: Prof. Shinsuke Shigeto

國立交通大學

應用化學系碩士班

碩 士 論 文

A Thesis

Submitted to M. S. program

Department of Applied Chemistry

College of Science

National Chiao Tung University

in Partial Fulfillment of the Requirements

for the Degree of Master of Science

in

Applied Chemistry

July 2013

Hsinchu, Taiwan

中華民國一百零二年七月

核鹼基模型化合物 4(3*H*)-嘧啶酮於溶液相的電場調變紅外線吸收光譜學

研究生：胡書瑋　　指導教授：重藤真介 博士

國立交通大學應用化學系碩士班

摘要

本論文中，作者利用電場調變紅外線吸收光譜學研究核鹼基模型化合物，4(3*H*)-嘧啶酮於溶液態對外加電場的反應。先前的文獻指出此化合物於溶液態將同時存在單體以及雙體，然而目前仍沒有實驗方法直接研究此化合物及其雙體的化學平衡。電場調變紅外線光譜學可靈敏地偵測分子對外加電場的反應。且已被證實為一種可研究在溶液相同時存在多物種系統的工具。本實驗為了同時偵測單體及雙體，主要研究碳氧雙鍵振動的波數區間且成功地偵測到約百萬分之一的吸收值變化。為了獲得定量的分子資訊， 我們量測一系列的角度χ相關實驗，χ為外加電場以及紅外線的電場極化向量的夾角。實驗結果與先前研究過的極性分子系統相當不同，此分子並無出現明顯的角度相關性。 為了更仔細的檢視角度相關實驗的結果，我們利用特徵值分解分析(SVD)成功將光譜分解為角度相關以及角度無關兩個成分。於角度無關成分中並沒有發現到原本預期的單雙體平衡訊號。原因可能是電場對極性分子(單體)的穩定能並不足夠使以分子間氫鍵結合的雙體(若為平面則無偶極矩)分離。角度相關成分對於原光譜的貢獻度比起先前研究過的極性分子不尋常的小，我們認為其原因是振動躍遷偶極與偶極矩的夾角相當接近會讓轉動極化訊號(於先前發表的文獻中通常是最主要的貢獻)消失的 54.7°(魔術角度)。據我們所知，本研究應是第一個研究核鹼基模型化合物 4(3*H*)-嘧啶酮在室溫溶液態對外加電場反應的實驗。

Infrared electroabsorption spectroscopic study of a nucleobase model compound 4(3*H*)-pyrimidinone in solution

Student: Shu-Wei Hu Advisor: Prof. Shinsuke Shigeto

M. S. Program, Department of Applied Chemistry

National Chiao Tung University

Abstract

In this thesis, 4(3*H*)-Pyrimidinone, an important model compound of pyrimidine base, in *p*-dioxane solution was studied with infrared (IR) electroabsoprtion spectroscopy. A previous study using FT-IR spectroscopy showed that the monomer and dimer of 4(3*H*)-pyrimidinone, coexist in the solution phase. Although it is crucial to understand the effects of an electric field on this molecule with respect to molecular structure and monomer–dimer equilibrium, direct experimental studies are yet to be done.

IR electroabsorption spectroscopy can detect the molecular responses to an externally applied electric field with high sensitivity. In particular, it has been proven a powerful technique for studying solution sample in which different molecular species coexist. We measured IR electroabsorption (ΔA) spectrum in the C=O stretching region of 4(3*H*)-pyrimidinone in *p*-dioxane in which both monomer and dimer appear. In a series of χ-dependent ΔA spectra, we did not observe marked χ dependence of the ΔA signals of both monomer and dimer. Here, angle χ is the angle between the direction of the applied field and the electric field vector of the IR light. To examine the χ-dependence of the ΔA spectra quantitatively, we performed singular value decomposition (SVD) analysis, in which the whole set of the spectra were decomposed into the χ-dependent and χ-independent spectral components. The χ-independent component, shows the prominent electronic polarization signal in contrast to other molecular liquids studied before. In addition, the ΔA signal arising from equilibrium change between the monomer and dimer was not observed in the χ-independent component, which implies that the dipolar stabilization with the applied electric field (~10MVm^{-1}) may not be strong enough to dissociate the dimer. The absence of a large χ dependent component is rather unusual for a polar molecule having a permanent dipole moment. We attribute this observation to the angle between the vibration transition moment and the permanent dipole moment which is very close to the magic angle 54.7°, at which the orientational polarization signal vanishes. Results of our least-squares fitting

analysis of the χ-dependent spectral component are consistent with our interpretation. The present IR electroaborption study of 4(3*H*)-pyrimidinone has revealed experimentally for the first time the electric-field effects of a nucleobase model in a biologically relevant environment (i.e., ambient solution).

Acknowledgments

首先，我想感謝的人是我的指導教授重藤真介。他給予一個學風自由，不做無謂限制的研究環境，並總是樂於和學生討論解決未知的難題，當我有缺失時也會立刻提醒我。

接著，如果沒有史習岡、黃鎮遠、Hemanth、Sudhakar 這幾位學長的幫忙這本論文是無法完成的。對於他們幾位，我無限感激。再來我想謝謝所有重藤實驗室的成員。重藤實驗室因為有你們總是有正面向上的氣息。我想特別感謝蔣富珉以及王政璿總是在我實驗遇到困難或瓶頸時跟我去喝下午茶聊天玩樂，王政璿還在百忙中抽空幫我搬家。真的很感謝你們。

再來我想感謝我的父親給予我經濟上的幫助讓我能專心於學業。我的母親即使 15 年前因為和父親離婚一直以來和我總是聚少離多但她一直給予我精神上的支持。最後，我很感謝虹儀總是默默地在背後支持我，陪我度過各個不論辛苦或快樂的日子。謝謝你們所有人。

Contents

Page

摘要 ..... **i**

Abstract ..... **ii**

Acknowledgments ..... **iv**

Contents ..... **v**

List of Figures and Tables ..... **vi**

Chapter I Introduction **1**

Chapter II Experimental **6**

II-1. Introduction 7
II-2. Sample cell 7
II-3. Experimental system 10

Chapter III Theoretical **16**

III-1. Introduction 17
III-2. Orientational polarization 17
III-3. Electronic polarization 22
III-4. Equilibrium shift 23

Chapter IV IR electroabsorption spectroscopic study of 4(3*H*)-pyrimidinone in *p*-dioxane **32**

IV-1. Introduction 33
IV-2. Methodology 35
IV-3. Results and discussion 38
IV-4 Summary and future perspective 44

References **58**

List of Figures and Tables

Page

Figure I-1. Chemical structure of 4(3*H*)-pyrimidinone and its dimer. 5

Figure II-1. Home-made sample cell for IR electroabsorption measurements. 12

Figure II-2. RC circuit equivalent to the sample cell. 13

Figure II-3. Experimental setup of infrared electroabsorption spectroscopy 14

Figure II-4. Schema of the AC coupled amplification method 15

Figure III-1. Spectral features observed in ΔA spectrum. (a) IR absorption band. (b) the zeroth derivative shape, (c) the first derivative shape, and (d) the second derivative shape of the IR absorption band. 25

Figure III-2. Coordinate system used in the derivation of the orientational polarization signal. α is the angle between $\boldsymbol{\mu}_\mathbf{p}$ and $\boldsymbol{\mu}_\mathbf{T}$. This figure corresponds to the $\alpha = 0°$ case. 26

Figure III-3. Coordinate system used in the derivation of the orientational polarization signal. α is the angle between $\boldsymbol{\mu}_\mathbf{p}$ and $\boldsymbol{\mu}_\mathbf{T}$. This figure corresponds to the $\alpha = 90°$ case. 27

Figure III-4. Angle χ between the applied electric field F and the electric field vector **e** of the IR probe light [1]. Note that χ can be determined by applying Snell's law $\left[n_1 \cdot \sin\theta_1 = n_2 \cdot \sin(90-\chi)\right]$. 28

Figure III-5. (a) Electric field effect in the vibrational ground state and excited states. (b) An absorption peak shifts to higher wavenumber (purple to green), and the resulting Δ*A* spectrum (red) exhibits a first derivative shape. 29

Figure III-6. (a) Electric field effect in the vibrational ground state and excited state. (b) An absorption peak shifts to lower wavenumber (purple to green), and the resulting Δ*A* spectrum (red) shows a first derivative shape. 30

Figure III-7. (a) Electric field effect on the distribution of the transition frequency from the vibrational ground to an excited state. (b) An absorption peak is broadened (purple to green),

and the resulting Δ*A* spectrum (red) shows a second derivative shape. 31

Figure IV-1. (a) Concentration dependent FT-IR spectra of 4(3H)-Pyr in p-dioxane at 12 different concentrations in the 1740−1640 cm−1 region. (b) Concentration dependence of the absorbance ratio (defined as $A_{1675\ cm-1}$ / $A_{1706\ cm-1}$). 46

Figure IV-2. Area intensities of the monomer and dimer bands as a function of total concentration. The solid line is the fitting result based on the model functions (Eqs. IV-5 and IV-6).....47

Figure IV-3. (a) Δ*A* spectra of 4(3H)-Pyr in *p*-dioxane (60 mM) measured with an applied voltage of 45, 55, 65, and 75V. (b) Absorption spectrum of 4(3H)-Pyr measured with a 50 μm path-length cell consisting CaF_2 windows.....48

Figure IV-4. Band area of the Δ*A* signals for the 1722−1700 (blue circles), 1700−1682 (red squares), and 1682−1658 cm^{-1} (green triangles) region as a function of the square of external electric field. Solid lines are a fit to a linear function having a zero intercept. 49

Figure IV-5. Three independent sets of the Δ*A* spectra of 4(3H)-Pyr in *p*-dioxane (60 mM) measured at χ = 55, 66, 76, 83, and 90°. 50

Figure IV-6. (a) Averaged χ-dependent Δ*A* spectra. (b) Plot of singular values obtained from the SVD of the averaged χ-dependent Δ*A* spectra shown in panel a. The components associated with the three largest singular values are denoted 1, 2, and 3. (c) Spectral components corresponding to the largest three singular values.....51

Figure IV-7. (a) Model functions (solid line) and reconstructed χ dependences (open triangles and circles). (b) χ-dependent (blue) and χ-independent (red) spectral components. 52

Figure IV-8. Observed (solid line) and reconstructed (dotted line) Δ*A* spectra of 4(3H)-Pyr in *p*-dioxane measured at χ = 55, 66, 76, 83, and 90°. 53

Figure IV-9. (a) IR absorption spectrum, the same as in Fig. IV-2(b). Also shown is the best fit to a sum of two Gaussian functions representing the C=O stretch bands of the monomer and the dimer of 4(3H)-Pyr. (b) χ-dependent (triangles) and χ-independent (squares) spectral

components, and the best fit (solid curve) to a superposition of the zeroth, first, and second derivatives of the absorption bands. 54

Figure IV-10. Decomposition of the fitted results in Fig. IV-8 into the zeroth, first, and second derivative components: (a) χ-independent and (b) χ-independent components. (c) Fitted result of the absorption spectrum. 55

Figure IV-11. Predicted direction of the transition moment from the experimental results and the optimized structure of 4(3H)-Pyr calculated at the RB3LYP/6-31+G(d,p) level. 56

Table I. Assignments, peak positions, and bandwidths of the two IR bands observed in the wavenumber region 1740−1640 cm^{-1}. 57

Table II. Coefficients a_χ, b_χ, and c_χ, of the zeroth, first, and second derivative terms of the absorption bands of 4(3H)-Pyr and its dimer. Note that $a_\chi = \Delta A/A$ and the absorbance A was taken from the spectrum measured with the 50-μm sample cell. 57

Table III. Stark parameters A_χ, B_χ, and C_χ. Note that f is the local field correction factor..... 57

Chapter I
Introduction

Fundamental properties of molecules such as chemical bonding and dipole moment are influenced profoundly by electrostatic interactions. Responses of molecules to an external electric field sharply reflect these molecular properties. An effect of an external electric field on absorption and emission spectrum is called the Stark effect. Stark spectroscopy is a general term describing the study of these responses to an applied electric field as changes in spectra. The terms electroabsorption, electro-optic absorption, and electrochromism have also been used in the literature to describe the same phenomenon.

This method provides unique information on molecular properties in diverse system ranging from an isolated gas-phase system to a complicated biological system and has been studied extensively in the visible region [1-3]. Liptay *et al.* have done a series of pioneering work [2, 4]. They not only demonstrated the experimental determination of electric properties of many aromatic molecules in solution but developed a theoretical basis of Stark spectroscopy, which is widely used in this area nowadays. Boxer *et al.* employed frozen glasses (at 77 K) to perform Stark spectroscopy of donor-acceptor polyenes, transition metal complexes (metal-to-ligand and metal-to-metal mixed valence transitions), and nonphotosynthetic biological systems [1, 5]. They discussed quantitatively the amount of charge transfer based on two characteristic parameters obtained directly from experiment: the change in dipole moment, $\Delta\mu$, and the change in polarizability, $\Delta\alpha$, between the ground and excited electronic states.

Ohta and co-workers used electroabsorption and electrofluorescence spectroscopy to study polymer films with specific dopant molecules [3, 6-8]. For example, they obtained the values of $\Delta\mu$ and $\Delta\alpha$ of two different dopants (2-hydroxyquinoline or 6-hydroxyquinoline) embedded in a polymer film through temperature dependence [6]. These parameters and properties are useful when developing and designing novel optical devices.

Vibrational Stark spectroscopy looks at vibrational transition instead of electronic transition. Compared to other spectral methods, vibrational spectroscopy is more sensitive to

molecular structure and local environments of molecules, as vibrational spectra are often called “molecular fingerprints”. Thus, vibrational Stark spectroscopy (infrared electroabsorption) provides more direct information on structural properties than its visible counterpart. However, there were much fewer electroabsorption spectroscopic studies in the infrared region in comparison to those in the visible, mainly due to experimental difficulty in detecting extremely small signals with a low-sensitivity IR detector.

To the best of our knowledge, the first infrared electroabsorption (IREA) spectroscopic study was reported by Handler and Aspnes in 1967 [9]. They investigated the OH stretch of 2,6-diisopropyl phenol in CCl_4 at room temperature and obtained the parameters associated with the dipole moment and the polarizability of the phenol. Nearly thirty years later, Chattopadhyay and Boxer studied the CN stretch of 4-methoxybenzonitrile in a toluene glass at 77 K and derived the parameters $\Delta\alpha$ and $\Delta\mu$. Since then, Boxer and co-workers extended their IREA studies in low temperature glass matrices [10]. In 2002, they applied the technique to free CO and CO bound to myoglobin (Mb). It is shown that the change in dipole moment for the CO bound to Mb is larger than that for the free CO because of d–π^* back-bonding [11]. Extensive studies from the Boxer group have recently been reviewed [12].

All these studies have been performed in liquid nitrogen glass matrices (77 K), where the reorientation of molecules is literally frozen or suppressed to a great extent [13]. The resultant electroabsorption (ΔA) spectra are more easily interpreted because the electronic response via $\Delta\alpha$ and $\Delta\mu$ are the only dominant contribution. However, these spectra are silent on molecular structure and association. In contrast, molecules having a permanent dipole moment in liquid/solution at room temperature undergo reorientation when an external field is applied, which gives rise to orientational polarization signal in the ΔA spectrum and provides rich structural information (see Chapter III for more details).

In 2001, Hiramatsu and Hamaguchi developed an IREA spectrometer that was intended for room temperature measurements and investigated the *trans*/*gauche* conformational

equilibrium of liquid 1,2-dichloroethane [14]. Instead of using the conventional FT-IR method, a dispersive IR monochromator equipped with an AC coupled amplifier was employed, and an absorbance change induced by an applied electric field as small as 10^{-7} was successfully detected. They applied their apparatus to study the self-association of *N*-methylacetamide in 1,4-dioxane [15], association forms of liquid crystal (5CB) at different temperatures [16], and solvated structure of *p*-nitroaniline in mixed solvent of acetonitrile (ACN) /CCl_4 [17].

In 2007, the whole setup of IREA spectrometer was transferred and reconstructed at NCTU by Shigeto and co-workers. Using the setup at NCTU, Shigeto *et al.* studied the *trans*/*gauche* conformational equilibrium and associated thermodynamic parameters of liquid 1,2-dibromoethane [18], solvated structures of *N*,*N*-dimethyl-*p*-nitroaniline in ACN/C_2Cl_4 [19], and anharmonic coupling of the CH-stretch and CH-bend vibrations of liquid chloroform [20]. In the present work, the author uses IREA spectroscopy to study the structure of an important model compound of pyrimidine base, 4(3*H*)-pyrimidinone and its dimer in *p*-dioxane solution in the C=O stretching region. Figure I-1. shows the chemical structure of 4(3H)-pyrimidinone.

The rest of this thesis is organized as follows. In Chapter II, the details of our IREA spectrometer and a home-made sample cell are outlined. Chapter III describes the theoretical basis of IREA spectroscopy. Major molecular responses to an externally applied electric field that contribute to IR absorbance changes are considered, and their mathematical expressions are derived. In Chapter IV, the IREA spectroscopic study of 4(3*H*)-pyrimidinone in dioxane solution is presented. The IREA spectra of 4(3*H*)-pyrimidinone measured at different χ angles (the angle between the electric field vector of IR light and the direction of the external electric field) show that there is no appreciable χ dependence for the signals of both monomer and dimer of 4(3*H*)-pyrimidinone. This rather unusual result suggests that the angle between transition moment and dipole moment may be very close to the magic angle 54.7° and that the dimer has a base pair-like hydrogen-bonded structure.

Monomer

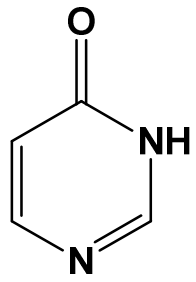

Dimer

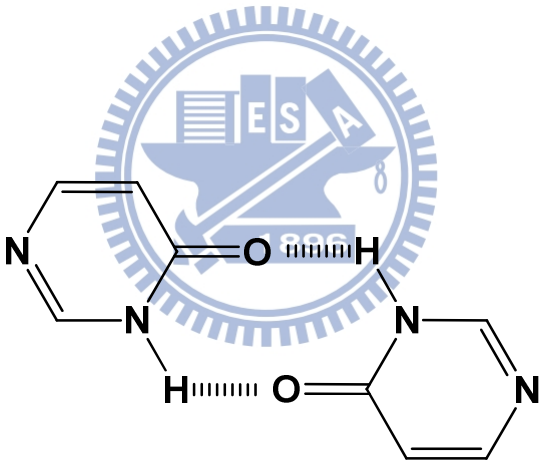

Figure I-1. Chemical structure of 4(3*H*)-pyrimidinone and its dimer.

Chapter II
Experimental

II-1. Introduction

Details and characteristics of the home-made sample cell and the measurement apparatus that are used in this study are described in this chapter

The main feature of the system is the use of an alternative-current (AC) coupled amplification and a dispersive IR monochromator [21-23], which enables one to measure the absorbance change (ΔA) induced by external electric field as small as 10^{-7}.

II-2. Sample cell

The information about the sample cell used in this study and some possible technical problems of this system are described in this section. Our home-made sample cell is based on the cell that was originally designed by Hiramatsu [14] so that one can flow the sample through it to avoid evaporation during measurement and apply an electric field across it.

Figure II-1 depicts the configuration of the cell. It consists of two brass cell holders (A/A'), a 6-μm-thick polyethylene terephthalate (PET) film spacer (C) sandwiched by two p-type boron-doped Si windows (B/B').

The PET film (Mitsubishi Plastic) must be thin enough to avoid applying high voltage. The Si plates (Pier Optics; thickness = 0.5 mm, resistivity = 0.8-2 Ω cm) also serve as electrodes. The surface contacting with the sample was coated by a SiO_2 layer (thickness = 0.3 μm, resistivity > 10^{10} Ω cm) for insulation. Chemically durable perfluoroelastmer O-rings were placed at between A' and B' to prevent the sample from leaking out of the cell.

To calculate the electric field strength applied across the sample, we need to estimate the cell gap accurately. We can do so by looking at an interference fringe pattern in the absorption spectrum of the empty cell. The cell gap g (μm) is related to the peak positions of two adjacent peaks of an interference fringe pattern, ω_1 and ω_2 (cm^{-1}) as:

$$2n_{\omega_1}g = \frac{2m-1}{2}\times\frac{10^4}{\omega_1} \quad \text{(II-1)}$$

$$2n_{\omega 2}g = \frac{2m+1}{2}\times\frac{10^4}{\omega_2} \quad \text{(II-2)}$$

where $n_{\omega 1}$ and $n_{\omega 2}$ are refractive indices at ω_1 and ω_2, and m is an integer.

Setting $n_{\omega 1} = n_{\omega 2}$, the cell gap g (μm) can be obtained as:

$$g = \frac{1}{2} \times \frac{10^4}{\omega_2 - \omega_1} \tag{II-3}$$

Non-negligible contact resistance between A-B and A'-B' may result in a voltage reduction between A-B (V_{AB}) and A'-B' ($V_{A'B'}$). To suppress this problem, the surface of the Si plates were scratched at two points separated by ~2cm to remove naturally coated SiO_2 and to put In-Ga (Ga 40%) paste to those points. The resistance between the two points was measured to make sure that it was less than ~20 Ω.

An ideal sample cell shown in Figure II-1 behaves as a capacitor. However, this is not the case in reality. The resistance originating from the Si electrodes themselves and their contacts with the brass cell holder make the cell a RC-circuit [24] (Figure II-2).

Figure II-2 shows an RC circuit equivalent to the sample cell. R_1 and R_2 are the resistances between A and B and between A' and B', respectively, and C_C is the capacitance between the electrodes. This RC circuit causes an artificial frequency dependence of the ΔA signal. The voltage applied to the sample ($V_{BB'}$) and the phase retardation are given by [24]:

$$V_{BB'} = \frac{V_{AA'}}{\sqrt{1 + (\omega R C_c)^2}} \tag{II-4}$$

$$\text{Retardation} = \arctan\left(\omega R C_c\right) \tag{II-5}$$

respectively. Here, R ($R=R_1+R_2$) is the total resistance of the circuit, and ω is the angular frequency of the applied electric field. The phase retardation with respect to the applied sinusoidal AC voltage not only causes the nonzero out-of-phase ΔA signals but induces Joule heat, which causes thermal disturbance to the sample.

The problem becomes more severe as the $\omega R C_c$ term becomes larger. The capacitance C_C varies depending on the concentration and the dielectric constant of the sample. Thus, the

best way to suppress the problem is to reduce the resistance R as much as possible.

The magnitude of an externally applied electric field, F_{ext}, can be calculated from the applied voltage and the cell gap. However, F_{ext} is not the exact field strength that acts on the molecules in the sample. It is the local field F_{local} that is actually exerted on the molecules [1, 12, 19]. Therefore we need to consider the relation between the local and external electric fields. The local electric field F_{local} is related to the external field as:

$$F_{local} = f' \cdot f'' \cdot F_{external} \tag{II-6}$$

Here the factor f' is given by:

$$f' = \frac{1}{\sqrt{1+(\omega RC_C)^2}}\left[\frac{1}{\sqrt{1+(\omega RC_C)^2}} + i\frac{\omega RC_C}{\sqrt{1+(\omega RC_C)^2}}\right] \tag{II-7}$$

which accounts for the effect of the RC circuit that the sample cell may form, and f'' is the local-field correction. It is a difficult task to accurately estimate f' and f''.

According to Onsager's theory, the local-field correction is given by:

$$f'' = \frac{3\varepsilon_r}{2\varepsilon_r + 1} \tag{II-8}$$

where ε_r is the dielectric constant of the medium. By definition, ε_r takes on values from unity to infinity, resulting in f'' between 1.0 and 1.5. However, this theory is based on a simple model of intermolecular interactions and liquid structures, and there are many limitations to broad applications. Thus, the values of molecular properties that require estimation of the local-field correction have often been given in units of f''.

A more practical way to determine the product $f' \cdot f''$ would be to use the orientational polarization signal of a polar molecule with a known dipole moment as an internal signal standard [19].

II-3. Experimental system

The experimental system used in this study is introduced in this section. A block diagram of the measurement system is shown in Figure II-3. A ceramic IR emitter (JASCO) was used as the light source. A pair of elliptical mirrors was used to focus the infrared light onto the sample. An optical chopper (Stanford Research System Inc., SR540) was placed at the co-focus of two elliptical mirrors to generate a modulation of 250 Hz to the light source. The light source and the sample cell were put on each of the other foci. A function generator (IWATSU, FG-330) and a power amplifier (NF corp., NF-4010) were used to generate a 25 kHz sinusoidal AC voltage (~70$V_{0\text{-}p}$), which was applied across the sample cell ~6 μm thick, producing an electric field of ~10^7 Vm^{-1} inside the cell.

A dispersive IR spectrometer (JASCO, TRIR-1000, Littrow mounting) was used for the measurement, whose focal length is 200 mm and the F number is 5. Three gratings are available in this spectrometer; their line density is 300, 120 and 60 mm^{-1}, respectively. In the present study, the grating with a line density of 120 mm^{-1} was used. A liquid nitrogen-cooled HgCdTe (MCT) detector (New England Research Center, MPP12-2-J3) was used for mid-IR signal detection.

The AC coupling scheme is a technique to probe a small AC signal buried in large direct current (DC) background [Figure II-4(a)]. Typically, the AC (intensity change induced by an external field) and DC (intensity of the IR light) voltages generated by the detector in the IR electroabsorption spectrometer are 10^{-8} V and 10^{-1} V respectively. In the measurement, the MCT detector is AC-coupled to a low-noise preamplifier, which removes the DC background so that the output of the preamplifier contains only the AC component [Figure II-4(b)]. The AC component is amplified once again [Figure II-4(c)] by the main amplifier (NF Corp., NF-5307, gain=1~1000 variable), and then fed to a lock-in amplifier (Stanford Research System, SR844). Note that the signal we detect is proportional to F^2 (second-order Stark effect), and hence it appears at 50 kHz.

The optical chopper and the oscilloscope were used for the measurement of the DC component, i.e., IR absorption spectrum [Figure II-4(d)]. In single electroabsorption experiment, three spectra are measured; (1) the spectrum of the light source (I_0), (2) the spectrum of the light intensity that is passed through the sample without external electric field modulation (I), and (3) the spectrum of the intensity change induced by external electric field (ΔI). The absorption spectrum of the sample is calculated from (1) and (2) as:

$$A = -\log(\frac{I}{I_0}) \tag{II-9}$$

The intensity difference spectrum ΔI is converted to absorbance change (ΔA) by:

$$\Delta A = A_{on} - A_{off} = -\log(\frac{I_{on}}{I_0}) - [-\log(\frac{I_{off}}{I_0})] = -\log(1 + \frac{\Delta I}{I}) \tag{II-10}$$

Note that ΔI is equal to I_{on}–I_{off}, and I is identical to I_{off} . This way, the IR absorption spectrum and the IR electroabsorption spectrum are derived.

The combination of a dispersive IR spectrometer and the AC coupling method affords detection the absorbance change (ΔA) as small as 10^{-7}, which is hard to be reached by the conventional FT-IR method [25, 26].

FT-IR spectra shown in chapter IV were measured with JASCO FT-IR-6100 spectrometer using a sample cell composed of two CaF_2 windows and a lead spacer of 100 μm thick. Resolution was 4 cm^{-1}, and 64 runs were averaged for each FT-IR spectrum.

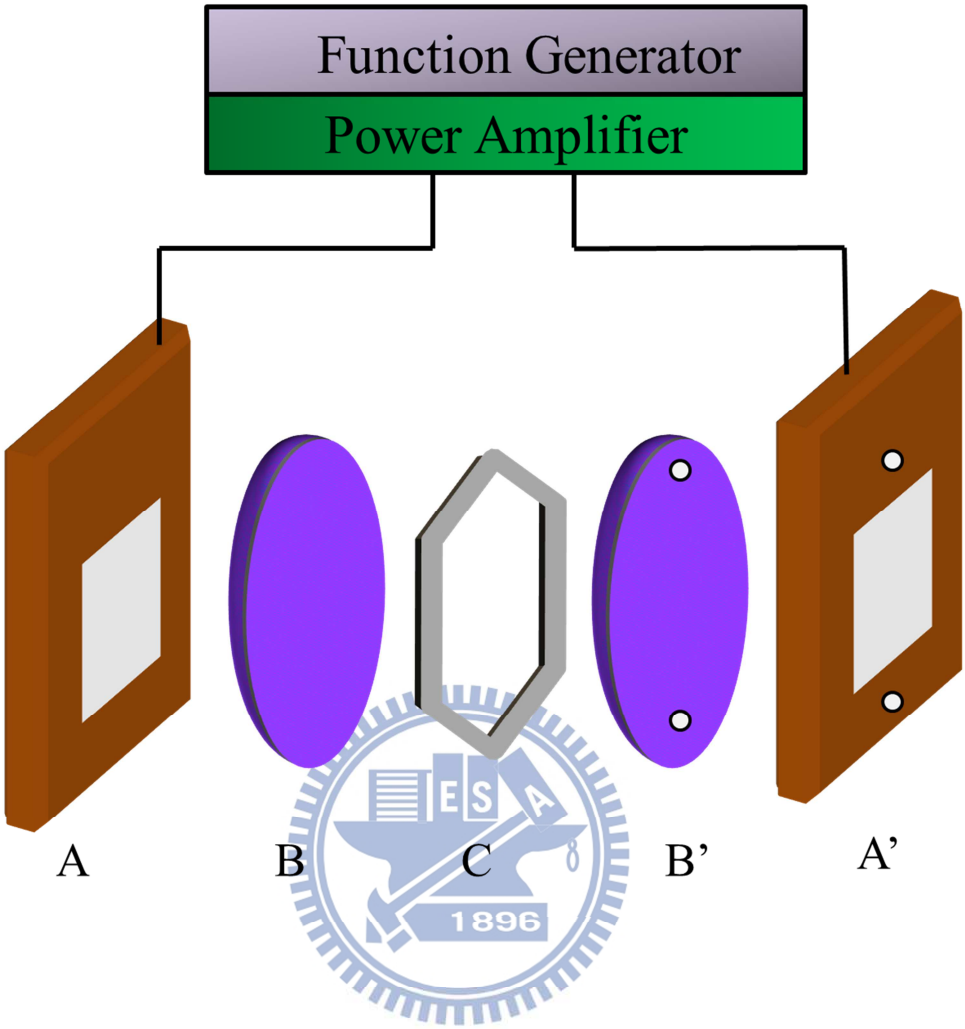

Figure II-1. Home-made sample cell for IR electroabsorption measurements. A, A': brass cell holders, B, B': Si windows/electrodes, C: PET film spacer [24].

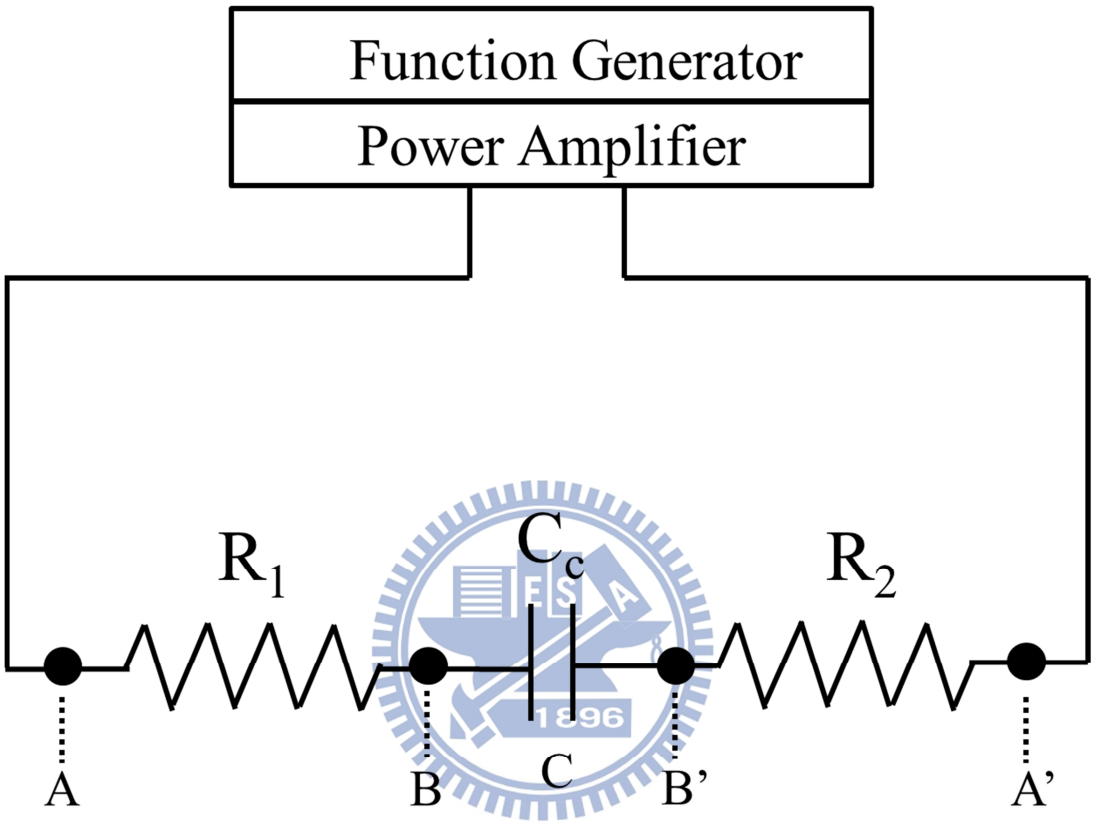

Figure II-2. RC circuit equivalent to the sample cell. R_1 is the resistance between A and B, R_2 the resistance between A' and B', and Cc the capacitance of the capacitor C [24].

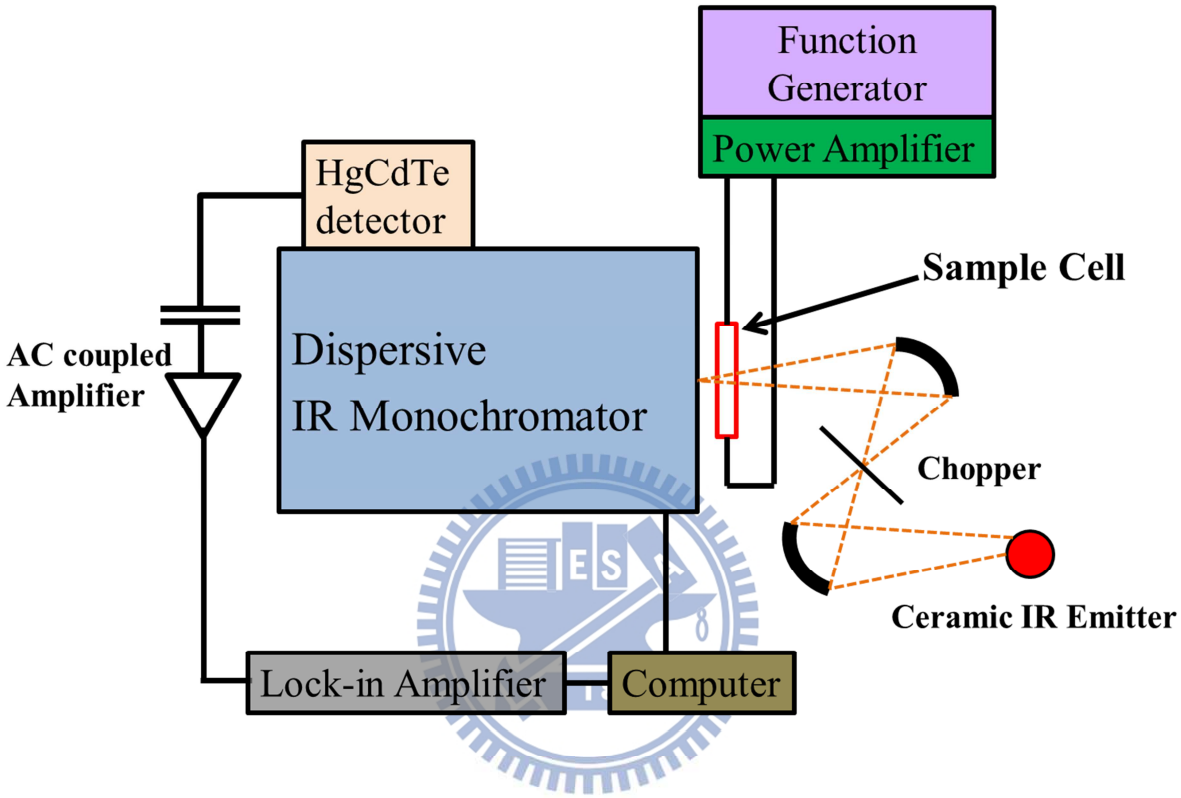

Figure II-3. Experimental setup of infrared electroabsorption spectroscopy [24].

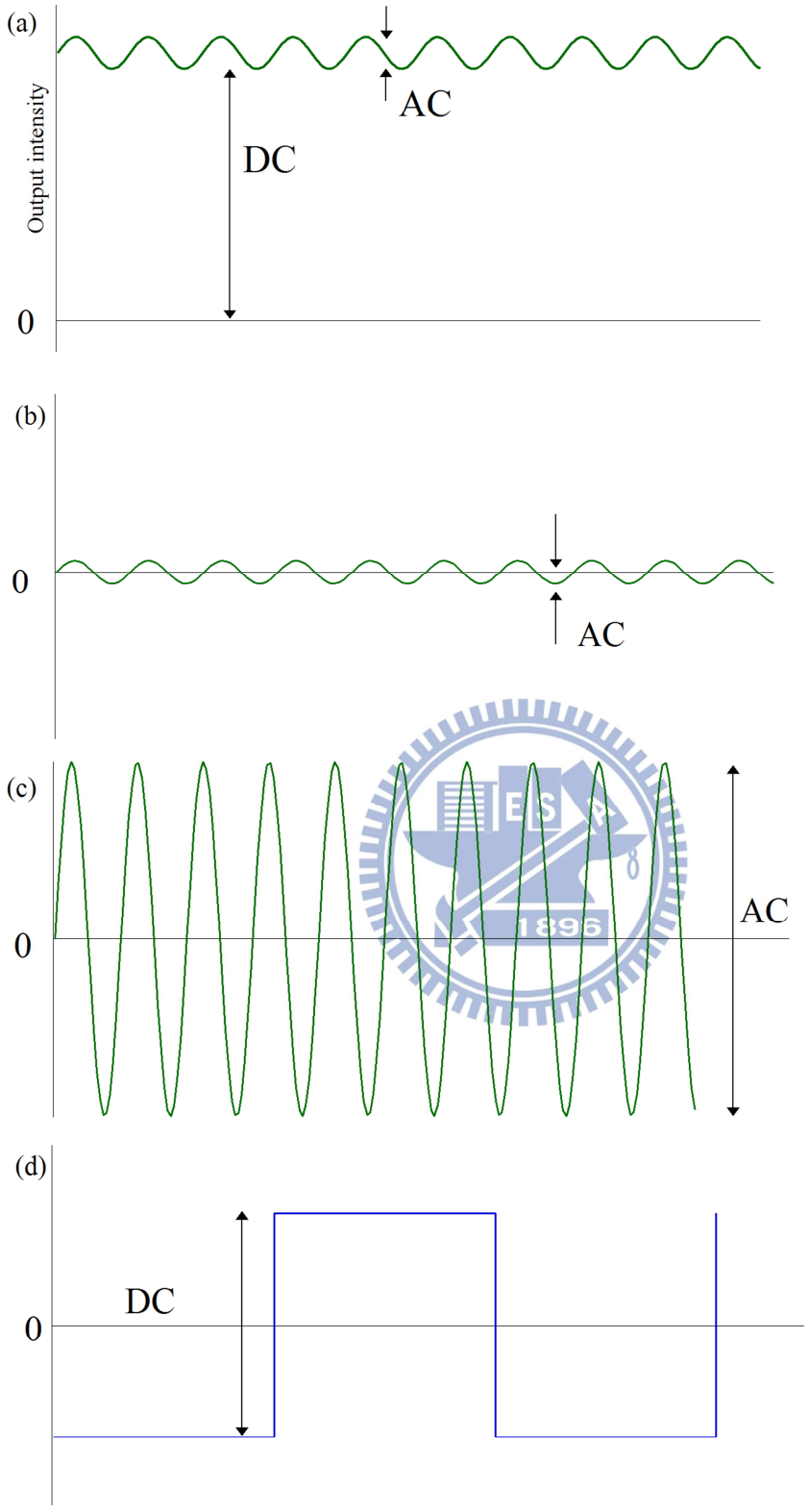

Figure II-4. Schema of the AC coupled amplification method

Chapter III
Theoretical

III-1. Introduction

The theoretical background and the formulations of several molecular responses to an external field observed in infrared electroabsorption (ΔA) spectra are introduced in this chapter. Three molecular responses are considered here, namely, the orientational polarization, the electronic polarization, and the equilibrium change [17, 24]. The ΔA signal originates from the changes in height, peak position, and width of an IR absorption band, and those changes appear in the ΔA spectra as the zeroth [Figure III-1(b)], the first [Figure III-1(c)], and the second [Figure III-1(d)] derivative shapes of the absorption band [Figure III-1(a)], respectively. The origins of these contribution seen in the ΔA spectrum are discussed.

III-2. Orientational polarization

When an external electric field is applied, liquid polar molecules having permanent dipole moment μ_p will orientate themselves so that their permanent dipole moment aligns parallel to the applied electric field [20, 24, 27]. It is known as an orientational polarization. The amplitude of the orientational polarization is a function of the permanent dipole moment of molecules. The orientational anisotropy induced in the sample gives rise to the absorbance change (ΔA).

In the following, the orientational polarization signal is formulated for (a) normally incident non-polarized IR light and (b) p-polarized IR light with tilt incidence, respectively.

(a) Normally incident non-polarized IR light

The orientational polarization signal ΔA can be derived starting from Beer-Lambert law:

$$\begin{aligned} A &= \varepsilon cl \\ &= cl \cdot K\tilde{\nu} \int_0^{\pi} \sin\theta d\theta \cdot f(\theta) \cdot \frac{1}{2\pi} \int_0^{2\pi} d\varphi \frac{1}{2\pi} \int_0^{2\pi} d\psi (\mathbf{e} \cdot \boldsymbol{\mu}_\mathbf{T})^2 \end{aligned} \tag{II-1}$$

where ε is the molar extinction coefficient, c the sample concentration (mol dm^{-3}), l the path length (cm) of the sample, K a constant, $\tilde{\nu}$ the wavenumber (cm^{-1}), and **e** a unit vector designating the direction of the electric field of the incident light. We set the molecule-fixed

coordinate system such that the *z*-axis coincides with the direction of the applied electric field and the propagation direction of the IR light as shown in Figures III-2 and III-3. The angles θ, ϕ, and φ determine the orientations of the dipole moment μ_p and the transition moment μ_T. A spatial distribution function $f(\theta)$, and the square of the scalar product of the transition moment and the unit vector $(\mathbf{e} \cdot \mu_T)^2$ are two integrands to be obtained explicitly. The distribution function

$f(\theta)$ is proportional to the probability of finding the dipole moment μ_p in the direction θ with respect to the applied electric field $\boldsymbol{F}$.

Using the coordinate system in Figures III-2 and III-3, we have

$$\boldsymbol{\mu_p} = \mu_p \begin{pmatrix} \sin\theta\cos\phi \\ \sin\theta\sin\phi \\ \cos\theta \end{pmatrix}, \quad \mathbf{F} = F \begin{pmatrix} 0 \\ 0 \\ 1 \end{pmatrix}, \quad \mathbf{e} = e \begin{pmatrix} \cos\psi \\ \sin\psi \\ 0 \end{pmatrix} \qquad \textbf{(III-2)}$$

The number of molecules that have energy E is proportional to $\exp(-\frac{E}{k_B T})$, and the energy E due to the dipolar interaction is given by

$$E = -\boldsymbol{\mu}_p \cdot \mathbf{F} = -\mu_p \begin{pmatrix} \sin\theta\cos\phi \\ \sin\theta\sin\phi \\ \cos\theta \end{pmatrix}^T \cdot F \begin{pmatrix} 0 \\ 0 \\ 1 \end{pmatrix} = -\mu_p F\cos\theta \qquad \text{(III-3)}$$

Thus the distribution function $f(\theta)$ becomes

$$f(\theta) = C\exp\left(\frac{\mu_p F\cos\theta}{k_B T}\right) = C\exp(\gamma\cos\theta) \qquad \text{(III-4)}$$

with

$$\gamma = \frac{\mu_p F}{k_B T} \qquad \text{(III-5)}$$

Here C is a normalization factor, T is the temperature, k_B is the Boltzmann constant, and F is the internal (not external) field strength. The parameter γ reflects the extent of the electrostatic interaction and in most cases plays a central role in the IREA spectroscopy of ambient polar liquid/solution.

The normalization factor C is determined by the condition

$$\int_0^{2\pi}\int_0^{\pi} f^{on}(\theta)\sin\theta d\theta d\phi = 1 \qquad \text{(III-6)}$$

In the presence of the electric field, $f(\theta)$ becomes from Eqs. III-4 and III-6

$$f^{on}(\theta) = \frac{1}{2\pi}\frac{\gamma}{\exp(\gamma)-\exp(-\gamma)}\cdot\exp(\gamma\cos\theta) \qquad \text{(III-7)}$$

In the absence of the electric field, we obtain $f(\theta)$ by taking the $\gamma\rightarrow 0$ limit of Eq. III-7

$$f^{off}(\theta) = \frac{1}{4\pi} \qquad \text{(III-8)}$$

The scalar product of μ_T and **e** can be calculated as follows. The electric field vector **e**, of the incident light lies in the xy-plane, and a projection of μ_T onto the xy-plane is related to $(\mathbf{e}\cdot\boldsymbol{\mu}_T)^2$. μ_T is thus expressed as

$$\boldsymbol{\mu}_T = |\mu_T|\cdot\begin{pmatrix} -\cos\phi\cos\theta\cos\varphi\sin\alpha-\sin\phi\sin\varphi\sin\alpha+\cos\phi\sin\theta\cos\alpha \\ -\sin\phi\cos\theta\cos\varphi\sin\alpha+\cos\phi\sin\varphi\sin\alpha+\sin\phi\sin\theta\cos\alpha \\ \sin\theta\cos\varphi\sin\alpha+\cos\theta\cos\alpha \end{pmatrix} \qquad \text{(III-9)}$$

If μ_P is parallel to μ_T, i.e., α=0° as shown in Fig. III-2, Eq. III-9 reduces to

$$\boldsymbol{\mu}_T = \mu_T\cdot\begin{pmatrix} \sin\theta\cos\varphi \\ \sin\theta\sin\varphi \\ \cos\theta \end{pmatrix} \qquad \text{(III-10)}$$

With the use of Eqs. III-2 and III-10, $(\mathbf{e}\cdot\mu_T)^2$ is obtained as

$$(\mathbf{e}\cdot\boldsymbol{\mu}_T)^2 = \frac{1}{2}\mu_T{}^2\sin^2\theta \qquad \text{(III-11)}$$

Here we replace $\cos^2\psi$, $\sin^2\psi$, and $\cos\psi\ \sin\psi$ by their mean values evaluated for the range $0\le\psi\le 2\pi$ (1/2, 1/2, and 1, respectively). In the absence of the electric field, the absorbance A^{off} for an $\alpha = 0°$ vibrational mode is calculated from Eqs.III-1, III-8, and III-11 as

$$\begin{aligned} A^{off} &\propto \int_0^{2\pi}\int_0^{\pi} f^{off}(\theta)\cdot\sin\theta\cdot\left|\mathbf{e}\cdot\boldsymbol{\mu}_T\right|^2 d\theta d\varphi \\ &= \frac{1}{4\pi}\cdot\frac{1}{2}\mu_T{}^2\int_0^{2\pi}\int_0^{\pi}\sin^3\theta\cdot d\theta d\varphi \\ &= \frac{1}{3}\mu_T{}^2 \end{aligned} \qquad \text{(III-12)}$$

Similarly, substitution of Eqs. III-7 and III-11 into Eq. III-1 results in the absorbance for the α=0° mode when the electric field is turned on

$$A^{\text{on}} \propto \int_0^{2\pi}\int_0^{\pi} f^{on}(\theta)\cdot\sin\theta\cdot\left|\boldsymbol{e}\cdot\boldsymbol{\mu}_{\text{T}}\right|^2 d\theta d\varphi$$
$$= \frac{1}{2}\mu_T{}^2\cdot\frac{\gamma}{(e^{\gamma}-e^{-\gamma})}\cdot\left[\frac{2}{\gamma^2}(e^{\gamma}+e^{-\gamma})-\frac{2}{\gamma^3}(e^{\gamma}-e^{-\gamma})\right] \qquad \text{(III-13)}$$

By expanding the exponential functions and retaining terms up to third-order in γ, we have

$$A^{\text{on}} \propto \frac{2}{\gamma^2+6}\cdot\mu_T{}^2 \qquad \text{(III-14)}$$

To confirm that this approximation is valid, suppose 50 V is applied across liquid acetone 5 μm thick. The electric field strength $F = 1\times10^7\ \text{V m}^{-1}$. For simplicity, we do not consider the local-field correction. Using the dipole moment of acetone, μ_{P} = 2.7 D (1 D = 3.33564 × 10^{-30} C m), we obtain γ= 0.02, for which γ<< 1 holds. The absorbance change caused by the applied electric field is the difference between A^{on} (Eq.III-14) and A^{off} (Eq.III-12). The absorbance change ratio is thus

$$\frac{\Delta A}{A^{off}} = \frac{A^{on}-A^{off}}{A^{off}} = -\frac{\gamma^2}{\gamma^2+6} \qquad \text{(III-15)}$$

Next we consider the α=90° case where μ_{p} is perpendicular to μ_{T} (Fig. III-3).

Equation III-9 reduces to

$$\boldsymbol{\mu}_{\mathbf{T}} = \mu_T\cdot\begin{pmatrix}-\cos\varphi\cos\theta\cos\phi-\sin\varphi\sin\phi\\-\sin\varphi\cos\theta\cos\phi+\sin\varphi\cos\phi\\\cos\phi\sin\theta\end{pmatrix} \qquad \text{(III-16)}$$

and $(\mathbf{e}\cdot\boldsymbol{\mu}_{\mathbf{T}})^2$ yields

$$(\mathbf{e}\cdot\boldsymbol{\mu}_{\mathbf{T}})^2 = \frac{1}{4}\mu_T{}^2(\cos^2\theta+1) \qquad \text{(III-17)}$$

Making use of Eqs. III-1, III-7, III-8, and III-17, we end up with the absorbance change ratio of the form

$$\frac{\Delta A}{A^{off}} = \frac{\gamma^2}{2(\gamma^2+6)} \qquad \text{(III-18)}$$

Generalization of Eqs. III-15 and III-18 to an arbitrary angle α is straightforward. The absorbance change for angle α can be decomposed into its parallel (α=0°) and perpendicular (α=90°) components as follows:

$$\Delta A_{\alpha} = \left(\frac{\Delta A}{A}\right)_{\alpha=0^\circ} \left|\mu_T \cos\alpha\right|^2 + \left(\frac{\Delta A}{A}\right)_{\alpha=90^\circ} \left|\mu_T \sin\alpha\right|^2 \qquad \text{(III-19)}$$

Substitution of Eqs. III-15 and III-18 into this equation yields the following expression for the orientational polarization signal probed with the normal incidence

$$\Delta A_{\alpha} = \frac{\gamma^2}{2(\gamma^2+6)}(1-3\cos^2\alpha)\cdot A \qquad \text{(III-20)}$$

Again γ^2 is considered exceedingly smaller than 6 in the present study, so the first term in the denominator of Eq.III-20 is safely neglected. Therefore we are left with

$$\frac{\Delta A_{\alpha}}{A} = \frac{\gamma^2}{12}(1-3\cos^2\alpha) \qquad \text{(III-21)}$$

(b) p-Polarized light with tilted incidence

So far we have considered the case where the electric field vector of the incident, non-polarized light on the *xy*-plane is parallel to the sample cell. In other words, χ is equal to 90°, where χ is the angle between the applied electric field ***F*** and the electric-field vector **e** of the incoming IR light (see Fig. III-4). When p-polarized light whose electric field vector **e** has only *x*-component is incident upon the sample with angle χ, the absorbance change ratio is given by [17]

$$\frac{\Delta A_{\alpha,\chi}}{A} = \frac{1}{12}\left(\frac{\mu_p F}{k_B T}\right)^2 \left(1-3\cos^2\alpha\right)\left(1-3\cos^2\chi\right) \qquad \text{(III-22)}$$

It should be noted that $\frac{\Delta A_{\alpha,\chi}}{A}$ shows the 1-3cos$^2\chi$ dependence and that the signal disappears if χ = 54.7° or α = 54.7°. Another important point is that the orientational ΔA spectrum is proportional to the absorption spectrum *A*, indicating that it is manifested as the zeroth derivative shape of the absorption spectrum. Furthermore, Eq. III-22 can be used to determine the dipole moment [14, 17, 19] or angle α experimentally [20].

III-3. Electronic polarization

An absorbance change also arises from electronic polarization, which is the change by an externally applied field in molecule's electronic properties such as the dipole moment and the polarizability. A general theory of the electronic polarization signal was established by Liptay *et al* [2, 4]. For a mobile molecule in solution, the electronic polarization signal is given by the following formula [28, 29]

$$\Delta A(\tilde{\nu}) = F^2 \left[A_\chi A(\tilde{\nu}) + \frac{B_\chi}{15hc}\tilde{\nu}\frac{d}{d\tilde{\nu}}\frac{A(\tilde{\nu})}{\tilde{\nu}} + \frac{C_\chi}{30h^2c^2}\tilde{\nu}\frac{d^2}{d\tilde{\nu}^2}\frac{A(\tilde{\nu})}{\tilde{\nu}} \right] \tag{III-23}$$

where h is Planck's constant and c is the speed of light. $\Delta A(\tilde{\nu})$ comprises the zeroth, first, and second derivatives of the absorption band $A(\tilde{\nu})$. The coefficients A_χ, B_χ, and C_χ are given by

$$\begin{aligned} A_\chi = {} & \left(3\cos^2\chi - 1\right)\left[\frac{{\mu_g}^2}{30{k_B}^2T^2}\left(3\hat{\mathbf{m}}-1\right) + \frac{1}{10k_BT}\left(\alpha_{gm} - \frac{1}{3}\Delta\alpha_g\right) \right] \\ & + \frac{1}{30|\mathbf{m}|^2}\sum_{ij}\left[10{A_{ij}}^2 - \left(3A_{ii}A_{jj} + {A_{ij}}^2\right)\left(1-3\cos^2\chi\right) \right] \\ & + \frac{1}{15|\mathbf{m}|^2}\sum_{ij}\left[10m_iB_{ijj} - \left(4m_iB_{ijj}\right)\left(1-3\cos^2\chi\right) \right] \\ & + \frac{1}{15|\mathbf{m}|^2k_BT}\sum_{ij}\left[10m_iA_{ij}\mu_{gj} - \left(1-3\cos^2\chi\right)\left(3m_iA_{ji}\mu_{gj} + 3m_iA_{jj}\mu_{gi} - 2m_iA_{ij}\mu_{gj}\right) \right] \end{aligned} \tag{III-24}$$

$$\begin{aligned} B_\chi = {} & \frac{5}{k_BT}\left(\boldsymbol{\mu}_g\cdot\Delta\boldsymbol{\mu}\right) + \frac{5}{2}\mathrm{Tr}\,\Delta\boldsymbol{\alpha} \\ & -\left(1-3\cos^2\chi\right)\left[\frac{1}{kT}\left(\boldsymbol{\mu}_g\cdot\Delta\boldsymbol{\mu}\right)\left(3\hat{\boldsymbol{m}}^2-1\right) + \left(\frac{3}{2}\Delta\boldsymbol{\alpha}_m - \frac{1}{2}\mathrm{Tr}\,\Delta\boldsymbol{\alpha}\right) \right] \\ & + \frac{1}{|\boldsymbol{m}|^2}\sum_{ij}\left[m_iA_{ij}\Delta\mu_j - \left(3m_iA_{ji}\Delta\mu_j + 3m_iA_{jj}\Delta\mu_i - 2m_iA_{ij}\Delta\mu_j\right)\left(1-3\cos^2\chi\right) \right] \end{aligned} \tag{III-25}$$

$$C_\chi = |\Delta\mu|^2\left[5 + (3\cos^2\chi - 1)(3|\hat{\mathbf{m}}|^2 - 1) \right] \tag{III-26}$$

Here $\Delta\boldsymbol{\mu}$ and $\Delta\boldsymbol{\alpha}$ denote the changes in permanent dipole moment and polarizability tensor between the vibrational ground state (g) and an excited state (e), respectively, i.e., $\Delta\boldsymbol{\mu} = \mu_e - \mu_g$ and $\Delta\boldsymbol{\alpha} = \alpha_e - \alpha_g$. $\hat{\mathbf{m}}$ is a unit vector in the direction of the transition dipole moment. α_{gm} and $\Delta\alpha_m$ are the components of the polarizability change along the direction of the transition dipole moment, i.e., $\alpha_{gm} = \hat{\mathbf{m}} \cdot \alpha_g \cdot \hat{\mathbf{m}}$ and $\Delta\alpha_m = \hat{\mathbf{m}} \cdot \Delta\alpha \cdot \hat{\mathbf{m}}$. **A** and **B** are the transition polarizability and transition hyperpolarizability, respectively, exhibiting the field dependence of the transition moment: $\mathbf{m(F)} = \mathbf{m} + \mathbf{A} \cdot \mathbf{F} + \mathbf{F} \cdot \mathbf{B} \cdot \mathbf{F}$.

As described earlier, the zeroth-derivative component represents the intensity change of the absorption spectrum. Note that the first term in the square brackets in Eq. III-24 corresponds to the orientational polarization contribution, which we already derived above. The first-derivative component depends on both $\Delta\boldsymbol{\mu}$ and $\Delta\boldsymbol{\alpha}$, and is responsible for the peak shift, as shown in Figs. III-5 and III-6. The second-derivative component, which is characterized solely by $\Delta\boldsymbol{\mu}$, shows the change in the bandwidth of the absorption spectrum (see Fig. III-7).

III-4. Equilibrium shift

An equilibrium shift caused by an external electric field will also contribute to the ΔA signal. If the stabilization due to the dipole interaction with the applied electric field differs among coexisting molecular species in the sample, the equilibrium will shift toward more stabilized species. A good instance for such an equilibrium shift is found in the *trans*/*gauche* isomerism of 1,2-dichloroethane [14]. The *gauche* conformer of 1,2-dichloroethane has a permanent dipole moment, and it will get stabilized by an applied electric field. On the other hand, the *trans* conformer is non-polar due to the presence of a center of symmetry, and it will not benefit stabilization via interaction with the applied electric field. Thus, the equilibrium shifts to the more stabilized gauche conformer. The IR absorption intensity of the *gauche* conformer is expected to increase, whereas that of the *trans* conformer is expected to decrease.

Note that because the equilibrium shift signal changes the intensity of the absorption band, a zeroth-derivative shape will be observed in the ΔA spectrum. The spectral shape of the equilibrium change signal is the same as the orientational polarization signal, but the equilibrium shift signal is χ-independent. So, one can differentiate these two signals by studying the χ-dependent ΔA spectra.

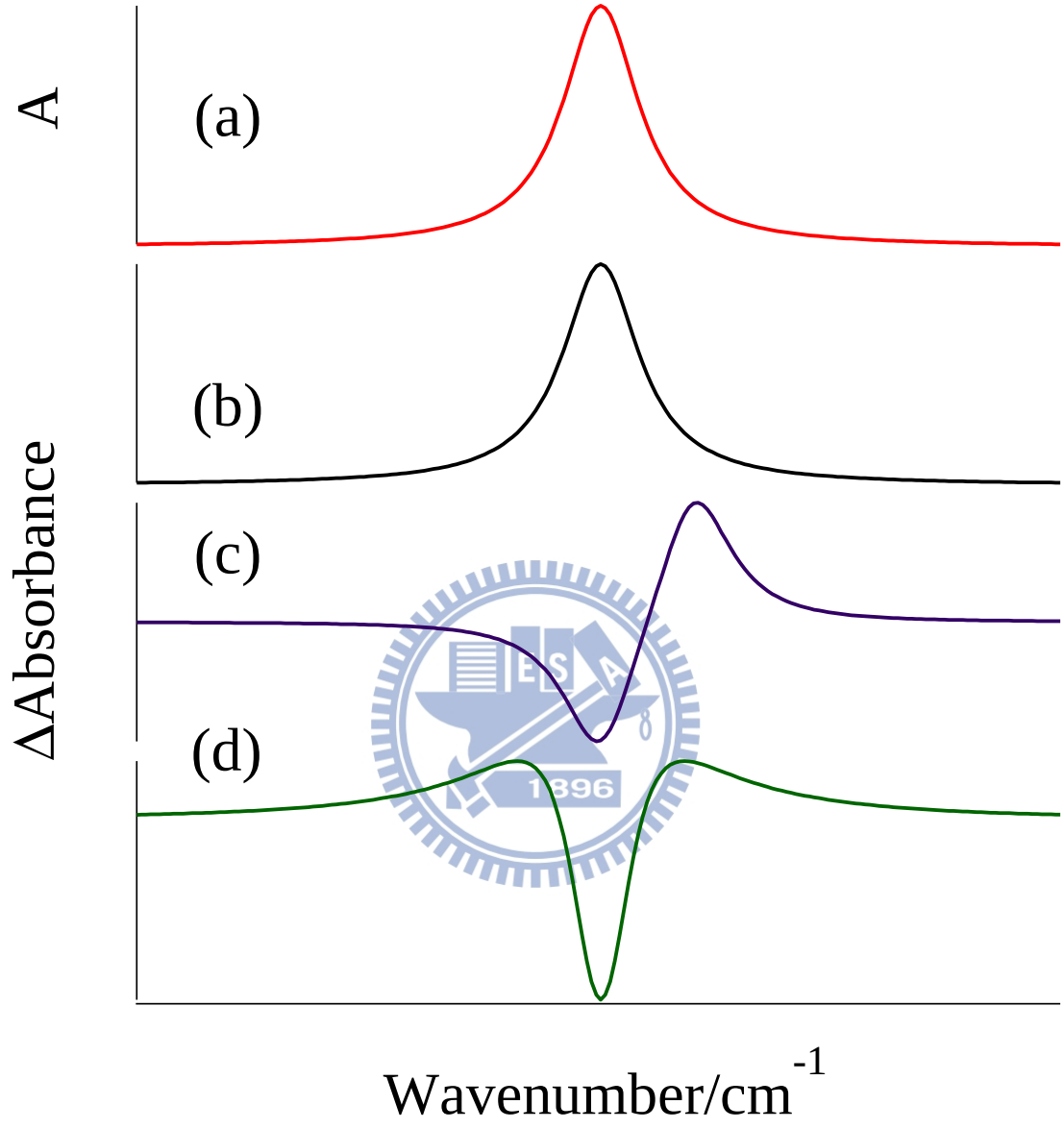

Figure III-1. Spectral features observed in ΔA spectrum. (a) IR absorption band. (b) the zeroth derivative shape, (c) the first derivative shape, and (d) the second derivative shape of the IR absorption band.

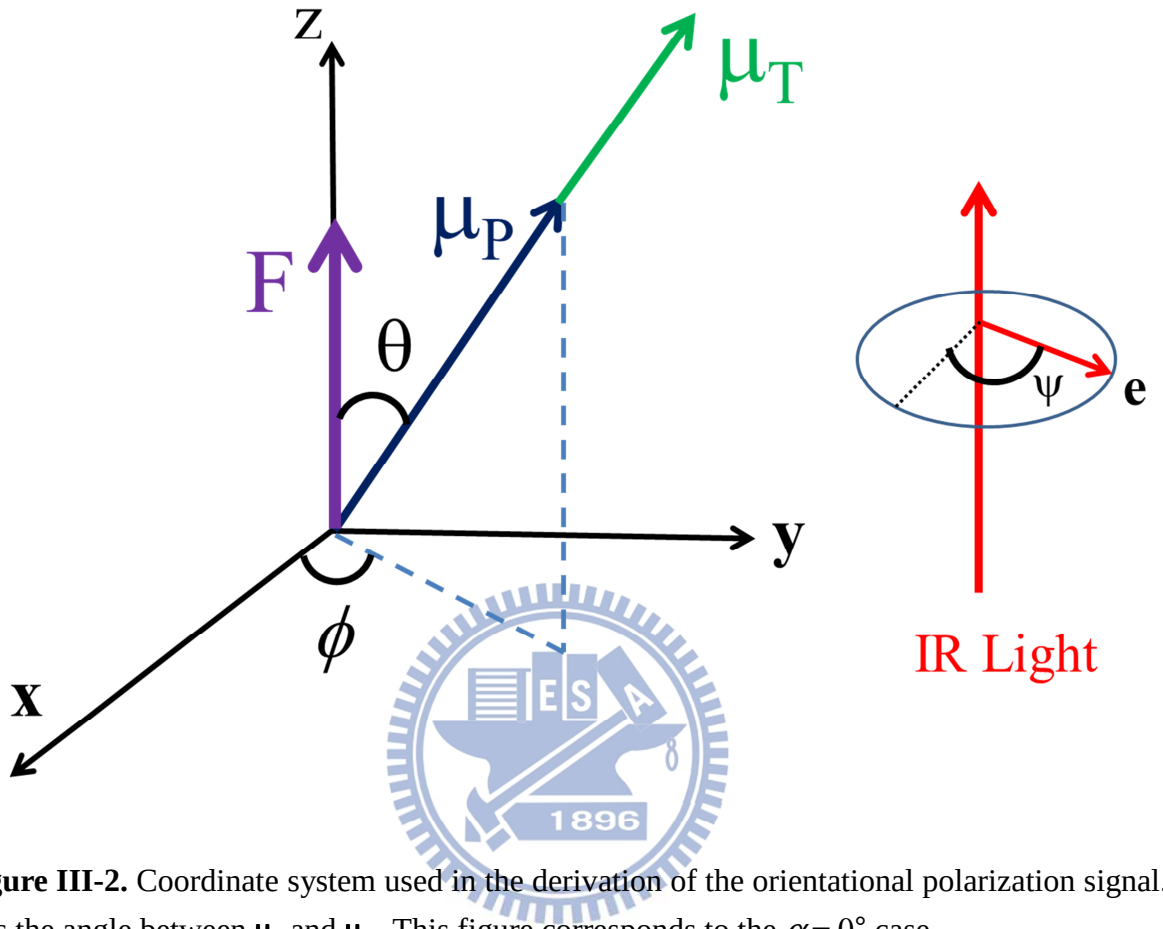

Figure III-2. Coordinate system used in the derivation of the orientational polarization signal. α is the angle between $\boldsymbol{\mu}_p$ and $\boldsymbol{\mu}_T$. This figure corresponds to the $\alpha = 0^\circ$ case.

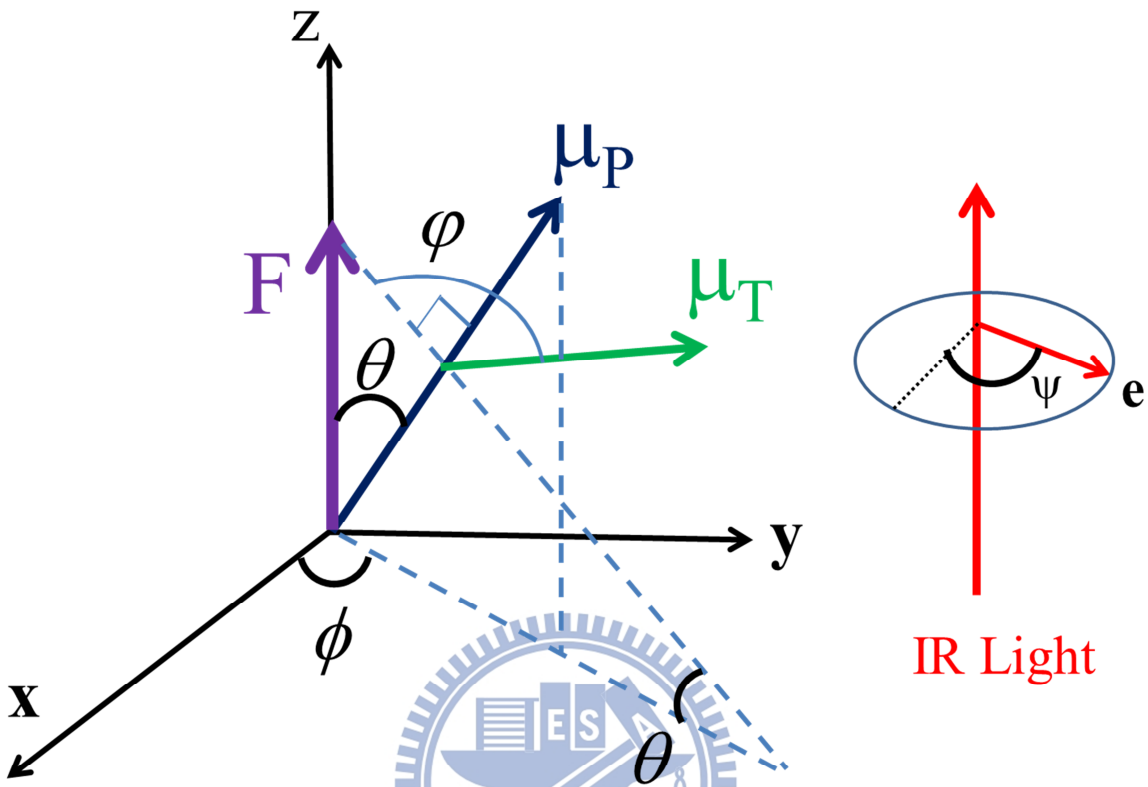

Figure III-3. Coordinate system used in the derivation of the orientational polarization signal. α is the angle between $\boldsymbol{\mu}_p$ and $\boldsymbol{\mu}_T$. This figure corresponds to the $\alpha = 90°$ case.

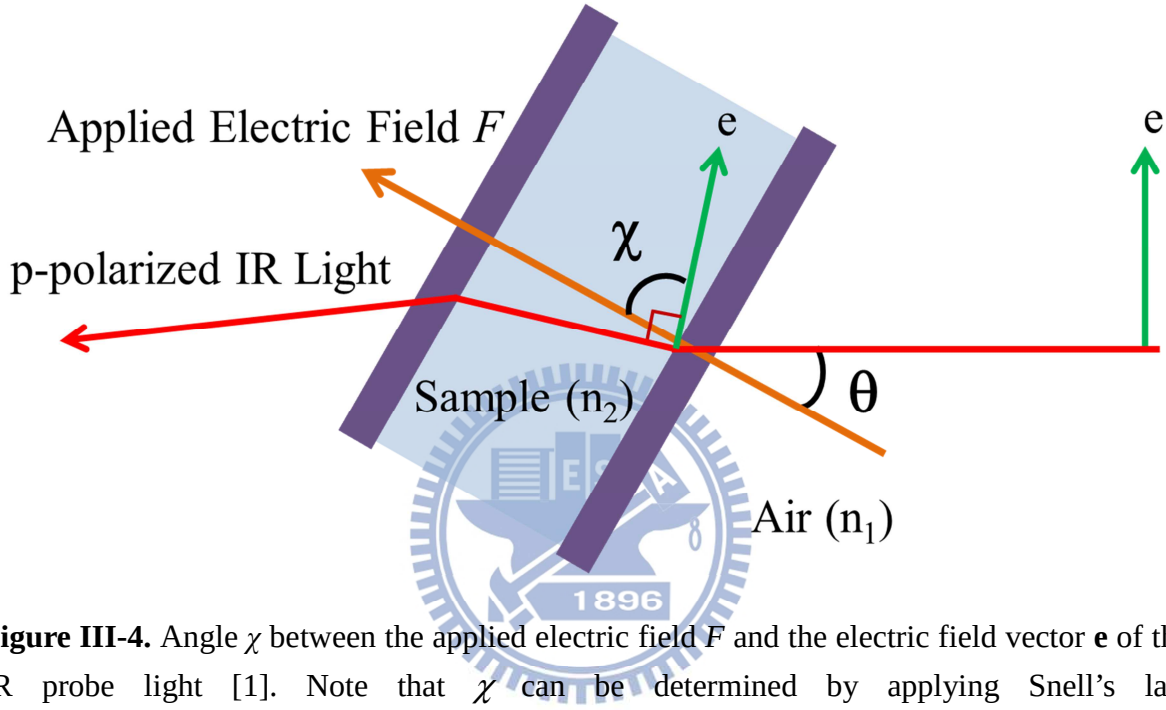

Figure III-4. Angle χ between the applied electric field F and the electric field vector **e** of the IR probe light [1]. Note that χ can be determined by applying Snell's law $\left[n_1 \cdot \sin\theta_1 = n_2 \cdot \sin(90-\chi)\right]$.

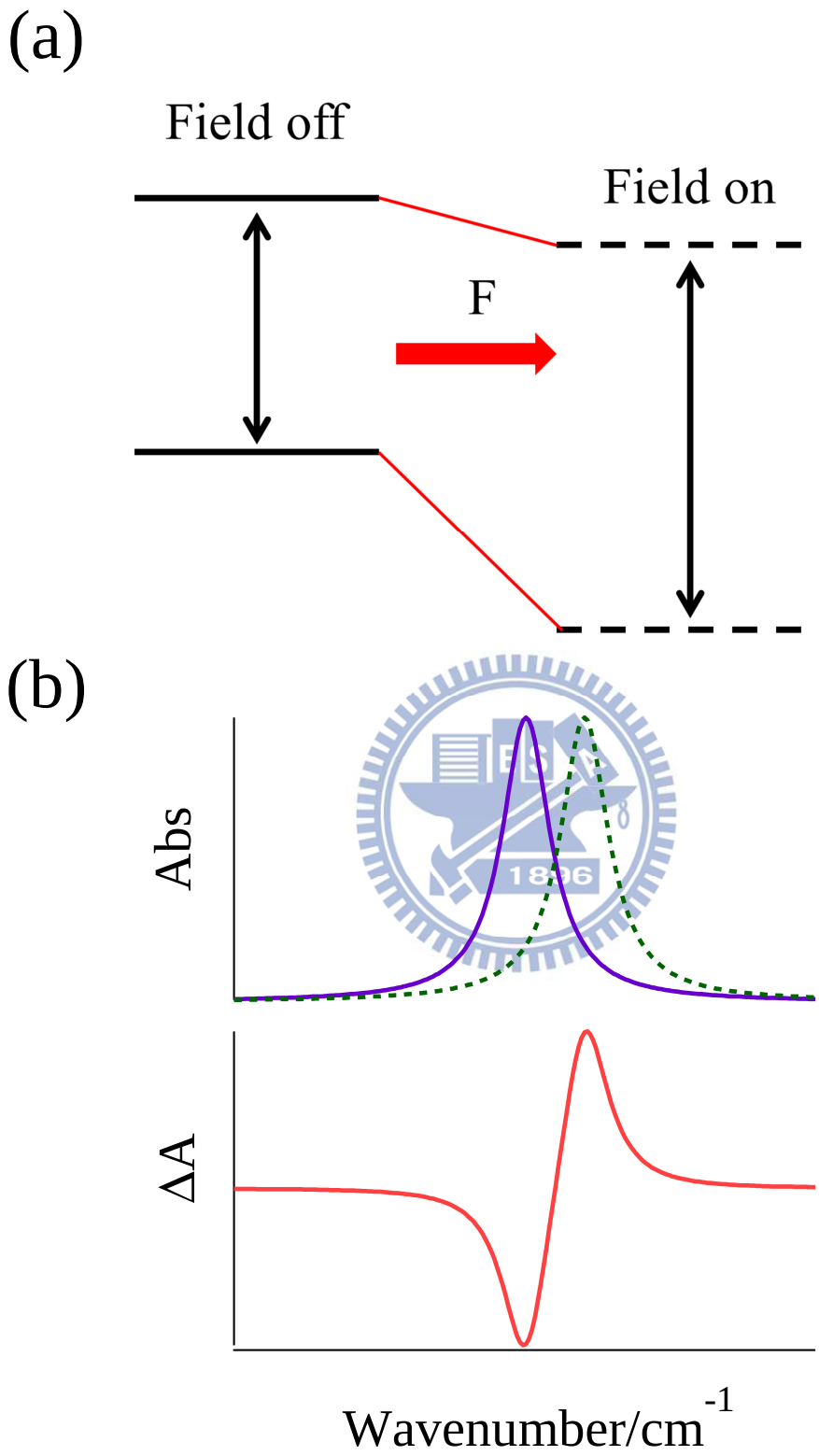

Figure III-5. (a) Electric field effect in the vibrational ground state and excited states. (b) An absorption peak shifts to higher wavenumber (purple to green), and the resulting Δ*A* spectrum (red) exhibits a first derivative shape.

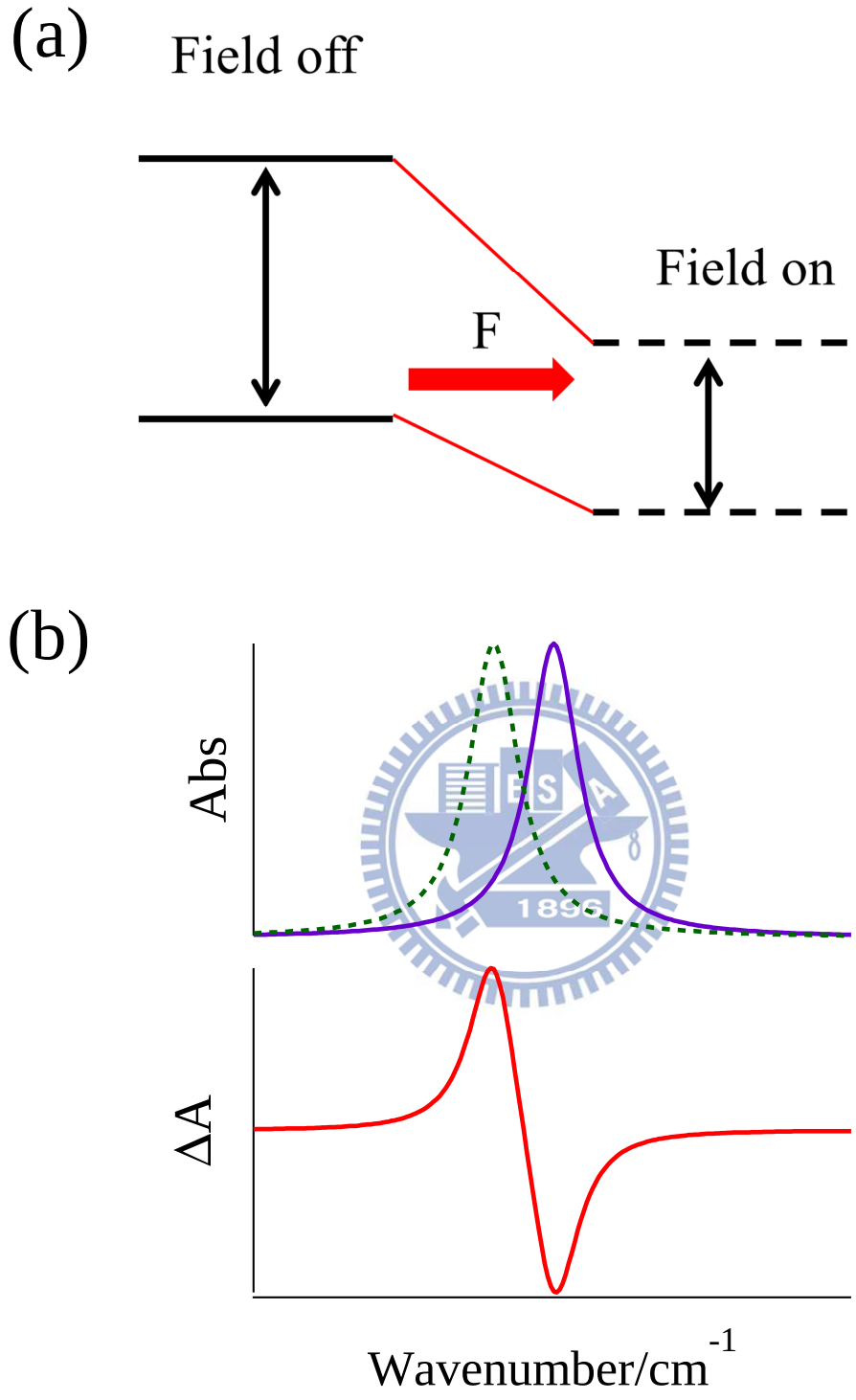

Figure III-6. (a) Electric field effect in the vibrational ground state and excited state. (b) An absorption peak shifts to lower wavenumber (purple to green), and the resulting Δ*A* spectrum (red) shows a first derivative shape.

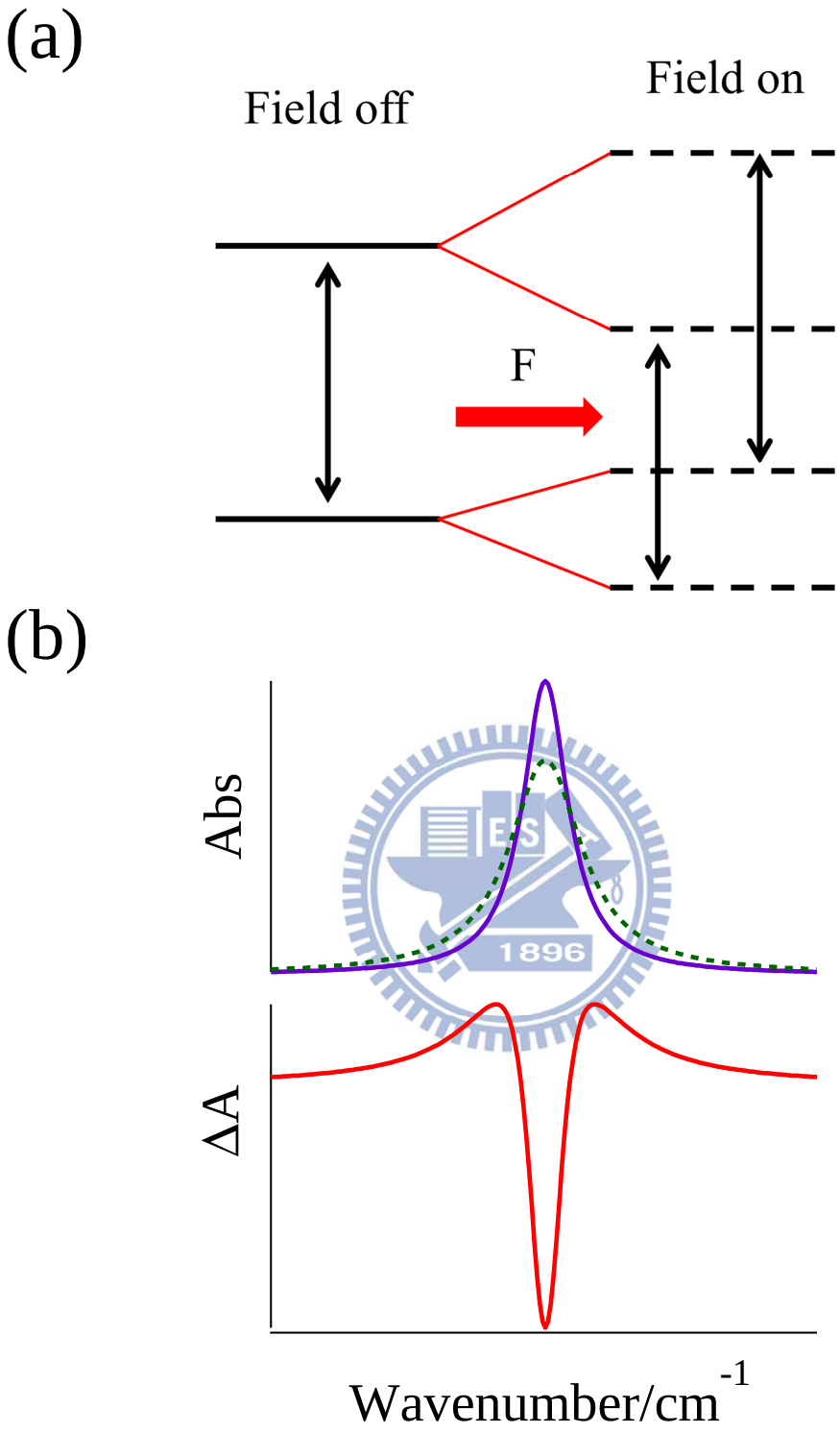

Figure III-7. (a) Electric field effect on the distribution of the transition frequency from the vibrational ground to an excited state. (b) An absorption peak is broadened (purple to green), and the resulting Δ*A* spectrum (red) shows a second derivative shape.

Chapter IV

Infrared electroabsorption spectroscopic study of 4(3*H*)-pyrimidinone in *p*-dioxane

IV-1. Introduction

The structure and the tautomerism of purine and pyrimidine nucleobases have been the focus of numerous experimental and theoretical studies [6, 27, 30-43]. This interest stems from their relevance to the important biological functions. For instance, the fidelity of DNA replication and transcription as well as the stabilization of secondary and tertiary structures of the nucleic acids are governed by specific hydrogen bonds between proper tautomeric forms of the complementary bases [44]. Vibrational spectroscopy is a powerful technique to investigate nucleobases and related compounds [38, 39, 45]. Changes in tautomerism, molecular structure, and hydrogen bonding state of the bases can be revealed by vibrational spectroscopy.

4(3*H*)-Pyrimidinone (4(3H)-Pyr) (Figure I-1) is a suitable model compound for studying nucleobases [40]. 4(3H)-Pyr exhibits a structure similar to that of the pyrimidine ring of the bases. Its keto and enol forms resemble the six-membered parts of the "normal" amino-oxo and "mutagenic" amino-hydroxy forms of guanine, respectively (see Figure I-1.). Knowledge of the tautomerism and structure of 4(3H)Pyr is therefore of considerable importance and is useful for gaining insight into the actual nucleobase systems. Previous studies suggested that the keto and the enol forms of 4(3H)-Pyr coexist in the gas-phase and low-temperature matrices in comparable amounts [35, 46]. In contrast, the keto form predominates in the condensed phase [46, 47]. A number of combined experimental and theoretical studies have been performed on 4(3H)-Pyr to predict their tautomeric stabilities and to establish vibrational assignments [35, 36]. Most studies of 4(3H)-Pyr have so far been performed in gas-phase or matrix-isolated conditions, in which little intermolecular interactions is present. In fact, these interactions play a central role in the physicochemical properties of the nucleobases. Scientific studies of 4(3H)-Pyr in the solution phase are limited mainly due to the poor solubility of this compound in less polar organic solvent. Aida *et al.* performed an IR spectroscopic study of 4(3H)-Pyr in chloroform and carbon tetrachloride solutions in combined with *ab inito*

calculations. They reported that the keto form of 4(3H)-Pyr monomer in the solution phase is dominant with an estimated tautomeric equilibrium constant K = 0.012, which was obtained from the absorbance ratio of the OH and NH stretch bands of the enol and keto forms, respectively. Furthermore, they discuss the molecular structures of keto-keto dimers coexisting with monomer [40].

In this study, we try to shed more light on 4(3H)-Pyr by means of infrared electroabsorption (IREA) spectroscopy. IREA spectroscopy can probe the molecular responses to an applied electric field as changes in IR absorption intensities. It sharply reflects the molecular structure in terms of the dipole moment [15, 17, 24] and the thermodynamic parameters associated with chemical equilibria [14, 18]. To be more specific, if we can extract orientational polarization signal (Eq. III-22) from angle χ dependent IREA spectra (χ is the angle between the direction of the applied electric field and electric field vector of the IR probe light), we will be able to obtain the information about permanent dipole moment μ_p or angle α (the angle between vibrational transition moment and dipole moment) [20] of the monomer and dimer of 4(3H)-Pyr simultaneously. Another important issue we want to address is the equilibrium change (see Chapter III-4.) between the monomer and the dimer of 4(3H)-Pyr. The monomer has a permanent dipole moment of 2.72 Debye in *p*-dioxane [48], whereas the dipole moment of the dimer is zero if a planar base pair-like hydrogen bonded structure is assumed (Figure I-1). We expect that the equilibrium between the monomer and the dimer would shift to the monomer because it is polae and can be stabilized via dipolar interaction with an applied electric field.

In this study we have successfully obtained the IREA spectra of 4(3H)-Pyr at various angles. To our knowledge, the responses of a model compound of the pyrimidine base to an electric field have been measured for the first time at room-temperature. The observed IREA spectra show unusually small χ dependence. A further ananlysis using singular value decomposition (SVD) confirms that the χ-dependent component is indeed predominant in

4(3H)-Pyr. As opposed to our expectation, we do not see equilibrium change signal (i.e., a positive ΔA signal for the monomer, and a negative ΔA signal for the dimer). On the basis of results of a least-squares fitting analysis of the decomposed components, we discuss these findings in terms of the angle α and the contribution of electronic polarization.

IV-2. Methodology

IV-2-1. Experiment

The experimental apparatus and the sample cell used in this study have been described in Chapter II. To measure angle χ dependent ΔA spectra, a wire-grid IR polarizer (THORLABS, WP25H-C) was used to obtain p-polarized light (with respect to the silicon window). Fourteen scans were averaged for each ΔA spectrum, which required about two hours. The spectral resolution of IREA measurements was set to be 12 cm^{-1} to achieve higher signal-to-noise ratio (S/N). Care was taken in the sample flow through the cell in order to prevent heat accumulation and solvent evaporation.

FT-IR spectra were recorded on a JASCO FT-IR-6100 spectrometer using a sample cell composed of two CaF_2 windows and a lead spacer (100 μm thick). Resolution of 4 cm^{-1} was used, and 64 scans were averaged for FT-IR measurements. All experiments were performed at room temperature (293 K).

p-Dioxane (purity > 99.5%) was commercially obtained from J.T. Baker, and 4(3*H*)-pyrimidinone (purity > 98%) from Sigma-Aldrich. These chemicals were used as received. 4A molecular sieves were used to remove residual water in *p*-dioxane, followed by filtration (pore size: 0.2 μm) to remove dusts or unwanted particles in the stock solution.

To prepare the sample solution for IREA measurements, 0.0589g of 4(3*H*)-Pyr was weighted and added to a 10ml volumetric flask, which was then filled up with *p*-dioxane. An ultrasonicator was then used to dissolve 4(3*H*)-Pyr in the solvent (*p*-dioxane). The concentration of the sample solution for the IREA measurement was 60 mM.

IV-2-2. Analysis: Singular value decomposition

Singular value decomposition (SVD) is an important factorization method of a complex matrix. This technique can be employed in principal component analysis; thus it has found many applications in chemometrics and spectral analysis [14, 49, 50].

SVD is a mathematical technique to decompose an arbitrary matrix **M** ($m \times n$) into a product of three matrices, **U**, **W**, and **V** as

$$\mathbf{M} = \mathbf{U}\mathbf{W}\mathbf{V}^T \qquad \text{(IV-1)}$$

where **U** ($m \times n$) and **V** ($n \times n$) are normalized orthogonal matrices, and **W** ($n \times n$) is a diagonal matrix, whose diagonal matrix elements are called singular values. In the present study, a set of χ dependent infrared electroabsorption spectra can be regarded as the matrix **M**.

M is decomposed into the product of **U** (the angle χ-dependence), **W** (the singular value matrix) and **V** (the intrinsic spectral components) :

$$\begin{pmatrix} M_{11} & \cdots & M_{1n} \\ \vdots & \cdots & \vdots \\ M_{m1} & \cdots & M_{mn} \end{pmatrix} = \begin{pmatrix} U_{11} & \cdots & U_{1n} \\ \vdots & \cdots & \vdots \\ U_{m1} & \cdots & U_{mn} \end{pmatrix} \begin{pmatrix} w_1 & 0 & 0 \\ 0 & \ddots & 0 \\ 0 & 0 & w_n \end{pmatrix} \begin{pmatrix} V_{11} & \cdots & V_{1n} \\ \vdots & \cdots & \vdots \\ V_{n1} & \cdots & V_{nn} \end{pmatrix} \qquad \text{(IV-2)}$$

The row of **M** corresponds to the spectrum at a particular χ, and the column to the angle χ dependence at a particular wavenumber. The *i*th column of **U** gives the *i*th angle χ-dependence and the *i*th row of **V** gives the corresponding spectrum. The contribution of the *i*th component to the matrix **M** is expressed by the value of w_i, the *i*th diagonal element of the matrix **W**. Components of **U** and **V** associated with small singular values can be neglected because their contribution to the matrix **M** is negligibly small. Then the matrix **M** is reproduced by considering only those components of **U** and **V** matrices that are accompanied by large singular values. The number of large singular values gives the number of independent spectral components that show different χ-dependences.

In our experiment, two components are to be considered: one is the χ-independent (constant) component and the other is the χ-dependent component showing the $1-3\cos^2\chi$

dependence. Therefore, we confine our attention to the two largest singular values. In this case, Eq. IV-1 can be simplified to

$$\mathbf{M} = \mathbf{UWV}^T \approx (\mathbf{u}_1\ \mathbf{u}_2)\begin{pmatrix} w_1 & 0 \\ 0 & w_2 \end{pmatrix}\begin{pmatrix} \mathbf{v}_1 \\ \mathbf{v}_1 \end{pmatrix} \tag{IV-3}$$

Now that we are left with much reduced number of components, we can proceed to assign physical meaning to components 1 and 2. It should be noted that SVD is a purely mathematical operation and hence there are no physical meaning attached to vectors **u** and **v** as they stand. We need to reconstruct these vectors by taking a proper linear combination (represented by a 2×2 transformation matrix **K**) based on the model for the χ-dependence. Accordingly, the Eq. IV-3 is rewritten to

$$\mathbf{M} = \begin{pmatrix} \mathbf{u}_1 & \mathbf{u}_2 \end{pmatrix}\mathbf{K}^{-1}\mathbf{K}\begin{pmatrix} w_1 & 0 \\ 0 & w_2 \end{pmatrix}\begin{pmatrix} \mathbf{v}1 \\ \mathbf{v}2 \end{pmatrix} = \begin{pmatrix} \mathbf{u}_a & \mathbf{u}_b \end{pmatrix}\begin{pmatrix} \mathbf{v}_a \\ \mathbf{v}_b \end{pmatrix} \tag{IV-4}$$

where

$$\begin{pmatrix} \mathbf{u}_a & \mathbf{u}_b \end{pmatrix} = \begin{pmatrix} \mathbf{u}_1 & \mathbf{u}_2 \end{pmatrix}\mathbf{K}^{-1}$$

$$\begin{pmatrix} \mathbf{v}_a \\ \mathbf{v}_b \end{pmatrix} = \mathbf{K}\begin{pmatrix} k_1 & 0 \\ 0 & k_2 \end{pmatrix}\begin{pmatrix} \mathbf{v}_1 \\ \mathbf{v}_2 \end{pmatrix}$$

$$\mathbf{K} = \begin{pmatrix} k_1 & k_3 \\ k_2 & k_4 \end{pmatrix}$$

Constant coefficients k_1-k_4 can be determined by a least-squares analysis so that vectors $\mathbf{u}_a$ and $\mathbf{u}_b$ correctly represent the two angle χ-dependences of ΔA spectra, namely, constant and $1\text{-}3\cos^2\chi$. Using the transformation matrix **K** thus determined, vectors $\mathbf{v}_a$ and $\mathbf{v}_b$ are obtained which represent physically meaningful spectral components.

IV-3. Results and discussion

IV-3-1. Concentration dependent FT-IR spectra

First, to confirm the presence of both monomer and the dimer of 4(3H)-Pyr in our *p*-dioxane solution, we measured concentration-dependent FT-IR spectra of 4(3H)-Pyr in *p*-dioxane in the 1740–1640 cm^{-1} region at 12 different concentrations (5, 10, 15, 20, 25, 31, 35, 40, 45, 48.95, 55, and 62mM) [Figure IV-1(a)].

Two IR bands are observed in this wavenumber region, and the intensities of both bands increased with increasing the concentration of 4(3H)-Pyr. However, the extent of increase of these two bands is different. Figure IV-1(b) shows that the absorbance ratio (defined as the ratio of the absorbance of the lower-wavenumber band to that of the higher-wavenumber band) has a linear dependence with a positive slope on solute concentration. This result indicates that the increase of the lower-wavenumber band is greater than that of the higher-wavenumber band. Considering that the dimer is more abundant at higher concentrations, and that the intermolecular hydrogen bonding in the 4(3H)-Pyr dimer weakens the C=O bond, resulting in a red-shift of C=O stretch peak, this observation leads to a conclusion that the higher-wavenumber band arises from the monomer, and the lower wavenumber band from the dimer. This conclusion is consistent with the literature [40].

In addition, we developed a model describing the equilibrium between the monomer and dimer of 4(3H)-Pyr, in which the equilibrium concentration of the monomer (β) and dimer (α) can be formulated as follow:

$$\alpha = P\left(c + \frac{2}{K} - 2\sqrt{\frac{c}{K} + \frac{1}{K^2}} \right) \tag{IV-5}$$

$$\beta = Q\left(-\frac{2}{K} + 2\sqrt{\frac{c}{K} + \frac{1}{K^2}} \right) \tag{IV-6}$$

where c is the total concentration, K is the equilibrium constant defined as $K = \frac{\alpha}{\left(\beta/2\right)^2}$.

P and Q are the coefficients that account for the path length and the extinction coefficient.

To determine *K*, we carried out a least-squares fitting analysis on the area intensities of the monomer band and dimer band using Eqs. IV-5 and IV-6. Figure IV-2 plots the area intensities of both bands as a function of total concentration and the fitted results. The value of the equilibrium constant *K* is determined as 0.031±0.005, indicating the predominance of the monomer in the concentration range (5-62 mM).

IV-3-2. Electric field strength dependence of IREA spectra

Figure IV-3 shows the absorption spectrum and a series of Δ*A* spectra of 4(3H)-Pyr in *p*-dioxane measured with 45, 55, 65, 75 volts for the wavenumber region of 1740–1640 cm^{-1}. These voltages are equal to the strength of the external electric field of 9, 11, 13, and 15 MVm^{-1} respectively. The Δ*A* spectrum of pure *p*-dioxane was also measured at each voltage as blank experiment [dashed line in Fig. IV-3(a)] and turned out to be negligible, ensuring the spectral features seen in Δ*A* spectra of the solution (solid line) result from 4(3H)-Pyr. The absorption spectrum [Fig. IV-3(b)] has been solvent-subtracted and measured with a 50 μm path-length cell to achieve a higher S/N. The two IR bands obseved at 1706 cm^{-1} and 1675 cm^{-1} are assigned to the C=O stretching mode of the monomer and dimer of 4(3H)-Pyr as already discussed in Chapter IV-3-1 and in previous studies [40].

The Δ*A* spectra were measured with normally incident IR light (i.e., $\chi = 90°$). In the Δ*A* spectra, two negative features at ~1706 cm^{-1} and ~1675 cm^{-1} are observed, apparently corresponding to the absorption maxima of the monomer and dimer bands. However, the origin of a positive feature at around 1695 cm^{-1} is unclear because there seems no absorption band at this wavnumber. The origin of those Δ*A* signals will be discussed later (see Chpater IV-3-4).

As the external electric field strength increases, the Δ*A* signals become stronger while the overall shape remains unchanged. Figure IV-4 plots the band area of the Δ*A* signals estimated in the interval 1722–1700, 1700–1682, and 1682–1658 cm^{-1} , as a function of the square of

the external electric field strength, F_{ext}^2. The experimental data are fitted well to a straight line, ensuring that what we observed is the second-order Stark effect as mentioned in Chapter III.

IV-3-3. Angle χ-dependent IREA spectra

To clarify the origins of the distinct ΔA features, we measured a series of χ dependent ΔA spectra of 4(3H)-Pyr in *p*-dioxane. Figure IV-5 shows three independent sets of the angle χ-dependent IREA spectra of 4(3H)-Pyr in *p*-dioxane (external field strength ~ 12.5 MVm^{-1}) measured at five different angles χ = 55°, 66°, 76°, 83°, and 90° (normal incidence). The angle χ was calculated by taking into account the refractive index of the solvent (n=1.43 for *p*-dioxane). All the angle χ-dependent spectra shown in this thesis have been baseline-corrected. The variation in optical path length with angle χ was also corrected. Mere inspection of the three sets of ΔA spectra in Fig. IV-5 does not show any appreciable χ dependence. To examine the χ dependence of the spectra more closely, we performed SVD analysis of the data.

Before performing SVD, three sets of the data were first normalized to an averaged value of the ΔA signal at 1708 cm^{-1} to account for signal variation arising from different measurements and then averaged to achieve higher S/N. The averaged χ-dependent IREA spectra are displayed in Fig. IV-6(a). A plot of the singular values obtained from the SVD of this averaged dataset and the spectral components associated with the largest three singular values are shown in Figs. IV-6(b) and (c), respectively. Because the spectral component 3 is dominated by noise, we focus on the spectral components 1 and 2 when we reconstruct the physically meaningful spectral components (see Chapter IV-2-2). The χ dependences we obtained from Eq. IV-4 ($\mathbf{u}_a$ and $\mathbf{u}_b$) as well as the expected χ dependences (constant and $1-3\cos^2\chi$) are shown in Fig. IV-7(a). The corresponding spectral components ($\mathbf{v}_a$ and $\mathbf{v}_b$ in Eq. IV-4) are shown in Fig. IV-7(b). In Figure IV-8, the ΔA spectra reconstructed according to our model with Eq. IV-4 are compared with the observed spectra. The good agreement between the observed and reconstructed spectra verifies that the above SVD analysis is correct.

Hereafter, we discuss the least-squares fitting analysis of the IREA spectra on the basis of these decomposed spectra components.

IV-3-4. Least-squares fitting analysis of the IREA spectra

To decompose the χ-independent and χ-dependent ΔA spectra [Fig. IV-7(b)] into the distinct contributions described in Chapter III, we carried out a least-squares fitting analysis. First, the absorption spectrum [Fig. IV-3(b)] was fitted to a superposition of two Gaussian functions plus a baseline represented by an offset a:

$$A(\tilde{\nu}) = a + \sum_{i=1}^{2} B_i \exp\left[-\left(\frac{\tilde{\nu} - \tilde{\nu}_{0i}}{w_i} \right)^2 \right] \qquad \text{(IV-7)}$$

where B_i is the peak height, $\tilde{\nu}_{0i}$ the peak position, and w_i the bandwidth of the ith band (i = 1 or 2). The best fit is displayed in Fig. IV-9(a), and the peak assignments, the peak positions, and the bandwidths of the two bands so determined are summarized in Table I. With those bandwidths and peak positions fixed, the ΔA spectra were subsequently fitted to a linear combination of the zeroth, first, and second derivatives of each absorption band:

$$\Delta A(\tilde{\nu}) = a_\chi A(\tilde{\nu}) + b_\chi \tilde{\nu} \frac{d}{d\tilde{\nu}} \frac{A(\tilde{\nu})}{\tilde{\nu}} + c_\chi \tilde{\nu} \frac{d^2}{d\tilde{\nu}^2} \frac{A(\tilde{\nu})}{\tilde{\nu}} \qquad \text{(IV-8)}$$

which is essentially the same as Eq. III-23. Adjustable parameters in the fitting were the coefficients a_χ, b_χ, and c_χ of the derivatives for the monomer and the dimer IR bands of 4(3H)-Pyr. Figure IV-9(b) shows the fitted results of the χ-independent and the χ-dependent ΔA spectra. It is clear from Fig. IV-9(b) that the model function (Eq. IV-8) reproduces well both χ-independent and the χ-dependent ΔA spectra The decomposition of the fitted results into the zeroth, first, and second derivative components is shown in Fig. IV-10. The coefficients determined by the fitting are summarized in Table II. They are related to the coefficients, A_χ, B_χ, and C_χ in Eq. III-23 via the following equations:

$$a_\chi = F^2 A_\chi \tag{IV-9}$$

$$b_\chi = \frac{F^2}{15hc} B_\chi = \left(3.356\times10^{23}\right) F^2 B_\chi \tag{IV-10}$$

$$c_\chi = \frac{F^2}{30h^2c^2} C_\chi = \left(8.447\times10^{47}\right) F^2 C_\chi \tag{IV-11}$$

where F is the *internal* electric field strength. From the parameters a_χ, b_χ, and c_χ, the values of the molecular properties such as $\Delta\boldsymbol{\alpha}$, $\Delta\boldsymbol{\mu}$, and **A** can, in principle, be obtained using Eqs III-24-26. To do so, however, the local-field correction needs to be estimated (see below).

The IREA spectra of 4(3H)-Pyr show that the contribution of the χ-independent component is dominant over the χ-dependent component. This may not be surprising because we expect to observe equilibrium change (see Chapter III-4) between the monomer and dimer of 4(3H)-Pyr as the χ-independent component. If the equilibrium between the monomer and the dimer exists, an external electric field applied to the 4(3H)-Pyr molecule would cause a shift in the equilibrium in favor of the polar monomer. In that case, we should observe a significant positive ΔA signal for the monomer and a significant negative ΔA signal for the dimer. However, this prediction contradicts our IREA spectra, which exhibit a negative ΔA signal for both monomer and dimer [see zeroth derivative contribution shown in Fig IV-10(a)] This result implies that the stabilization due to the dipolar interaction between the dipole moment of the monomer and the external field (~10MVm^{-1}) may not be strong enough to dissociate the intermolecularly hydrogen-bonded dimer. Another possible origin of the zeroth derivative contribution to the χ-independent component is the electronic polarization. The significant contribution of the electronic polarization to the a_χ of the monomer is most likely a consequence of a large field dependence of the transition moment, i.e., transition polarizability **A**. In other words, the C=O stretching vibration of 4(3H)-Pyr is highly susceptible to the surrounding electrostatic environment, which is different from the case of acetone. The coefficients b_χ and c_χ of the 4(3H)-Pyr monomer and dimer can be attributed to electronic polarization. The b_χ term depends mainly on the interaction of the molecular

polarizability and the applied electric field. The c_χ term describes the interaction of $\Delta\boldsymbol{\mu}$ and the applied field. Detailed analysis of those electronic polarization contributions will require higher resolution measurements and it is left for future studies.

The most surprising result we found is that the orientational polarization, which is usually dominant for polar molecules [15, 17, 19], does not contribute much to the ΔA signal. Recall that the orientational polarization signal is χ-dependent (Eq. III-22). As discussed above, no appreciable χ-dependence was observed in a series of χ-dependent ΔA spectra, indicating that the contribution from the orientational polarization signal is small. We attribute this observation to angle α that is very close to the magic angle 54.7°. This hypothesis is discussed in the following paragraph.

4(3*H*)-Pyrimidinone has a permanent dipole moment of 2.72 D [48]. Therefore, according to Eq. III-22, if χ = 90° (i.e., normally incident IR light), a value of -1.68×10^{-6} or 8.4×10^{-7} for ΔA_{ori} is obtained, assuming that the angle α equals 0° or 90°, respectively (T= 293 K, A= 0.036, F_{ext} = 12.5 MVm^{-1}). Here, a value of 0.6 was used as the local-field correction factor, which is taken from the previous IREA work [24]. The assumption may be justified because the materials of our home-made sample cell and the solvent (*p*-dioxane) are the same as that work, and a very similar local-field correction factor should apply as well. The coefficient a_χ of the monomer obtained with the fitting analysis for the χ-dependent component is $a_\chi = (\Delta A/A)_{ori} = 5.7\times10^{-7}$.It is obvious from this value of a_χ that the angle α of 4(3H)-Pyr is neither 0° nor 90°. Using $(\Delta A/A)_{ori} = 5.7\times10^{-7}$ with Eq.III-22, we obtain α = 55.23°. The calculated result is consistent with our hypothesis that the angle α is very close to the magic angle 54.7° if the zeroth derivative contribution in the χ-dependent spectral component comes solely from orientational polarization. Figure IV-11 shows the optimized structure of 4(3H)-Pyr with a calculated dipole moment of 2.45 D and the direction of the vibrational transition moment predicted from our experimental results. The structural

optimization of 4(3H)-Pyr was performed using the DFT calculations with RB3LYP functional and the 6-31+G(d,p) basis set on Gaussian09.

For the dimer, too, no significant orientational polarization signal is observed as well [Fig IV-10(b)], suggesting that the structure of the dimer may resemble the base pair-like hydrogen bonded structure (Figure I-1.) as argued in the previous study [40].

IV-4 Summary and future perspective

In this thesis, the author has presented an IREA spectroscopic study of an important model compound of pyrimidine bases, 4(3*H*)-pyrimidinone in *p*-dioxane. To our knowledge, the IREA spectrum of 4(3H)-Pyr in room-temperature solution has been successfuly measured for the first time. The results have revealed that the angle between the transition moment of the monomer C=O stretch band and the permanent dipole moment is very close to 54.7°, at which the orientational polarization signal vanishes. We also found that a base pair-like hydrogen bonded structure is plausible for the dimer structure. Accurate knowledge on the direction vibrational transition moment directions in the molecule is important in spectral assignment [51, 52]. Especially in complex biological molecules, the problems associated with resolving vibrational bands arise, because the vibrational frequencies of various tautomers can be very similar [27].

For molecules possessing C_{2v} or higher symmetry, determination of the angle α is often obvious from the nature of the vibration. In contrast, for molecules of low-symmetry, the direction of vibrational transition moment directions are nontrivial and depends on the complicated motions that constitute the normal mode. Miller *et al.* developed an experimental method for determining the vibrational transition moment angle (VTMAs) using orientational polarization [27]. They applied this method to various biologically relevant compounds [31-33]. The molecules of interest are isolated in liquid helium nanodroplets, in which the molecules are cooled down to 0.37 K. In contrast, our IREA spectroscopy can measure the angle α in room-temperature liquids, which are much closer to a real biological system.

The present study has demonstrated the potential of our method to study biology-related molecules in more biologically relevant environments. The VTMAs and the dipole moment of association structures of base-pair model compounds can be obtained from IREA spectra simultaneously.

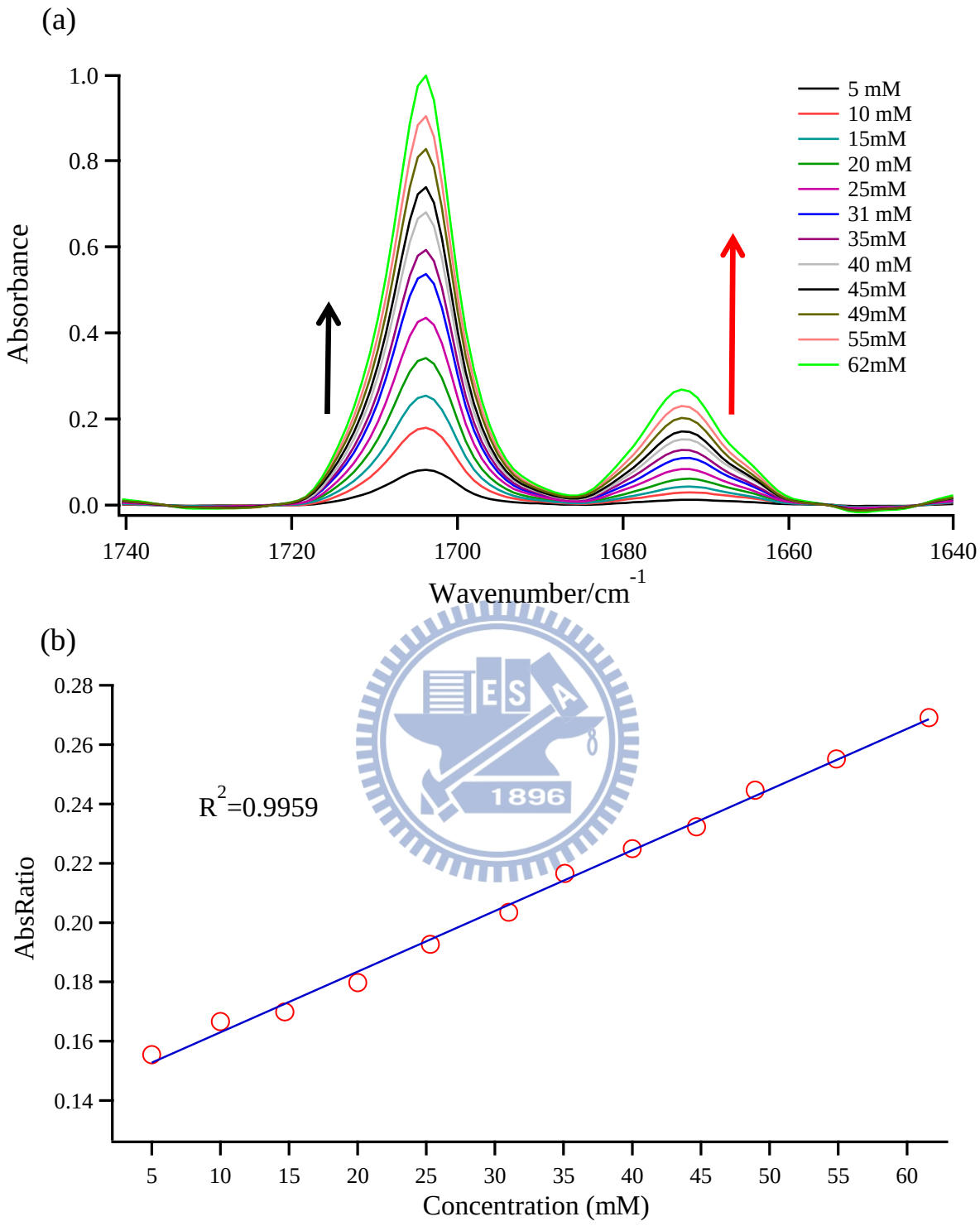

Figure IV-1. (a) Concentration dependent FT-IR spectra of 4(3H)-Pyr in p-dioxane at 12 different concentrations in the 1740−1640 cm−1 region. (b) Concentration dependence of the absorbance ratio (defined as $A_{1675\ cm-1}$ / $A_{1706\ cm-1}$).

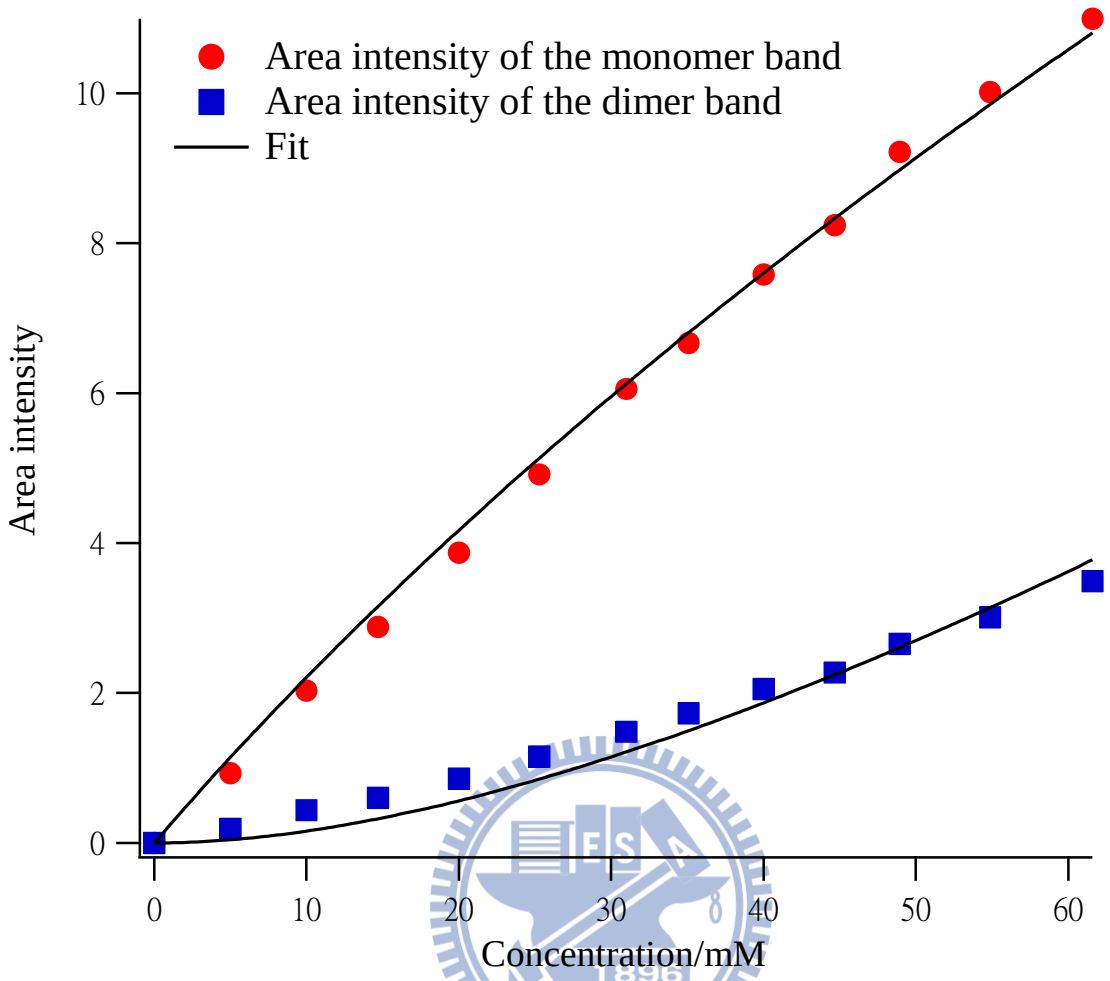

Figure IV-2. Area intensities of the monomer and dimer bands as a function of total concentration. The solid line is the fitting result based on the model functions (Eqs. IV-5 and IV-6).

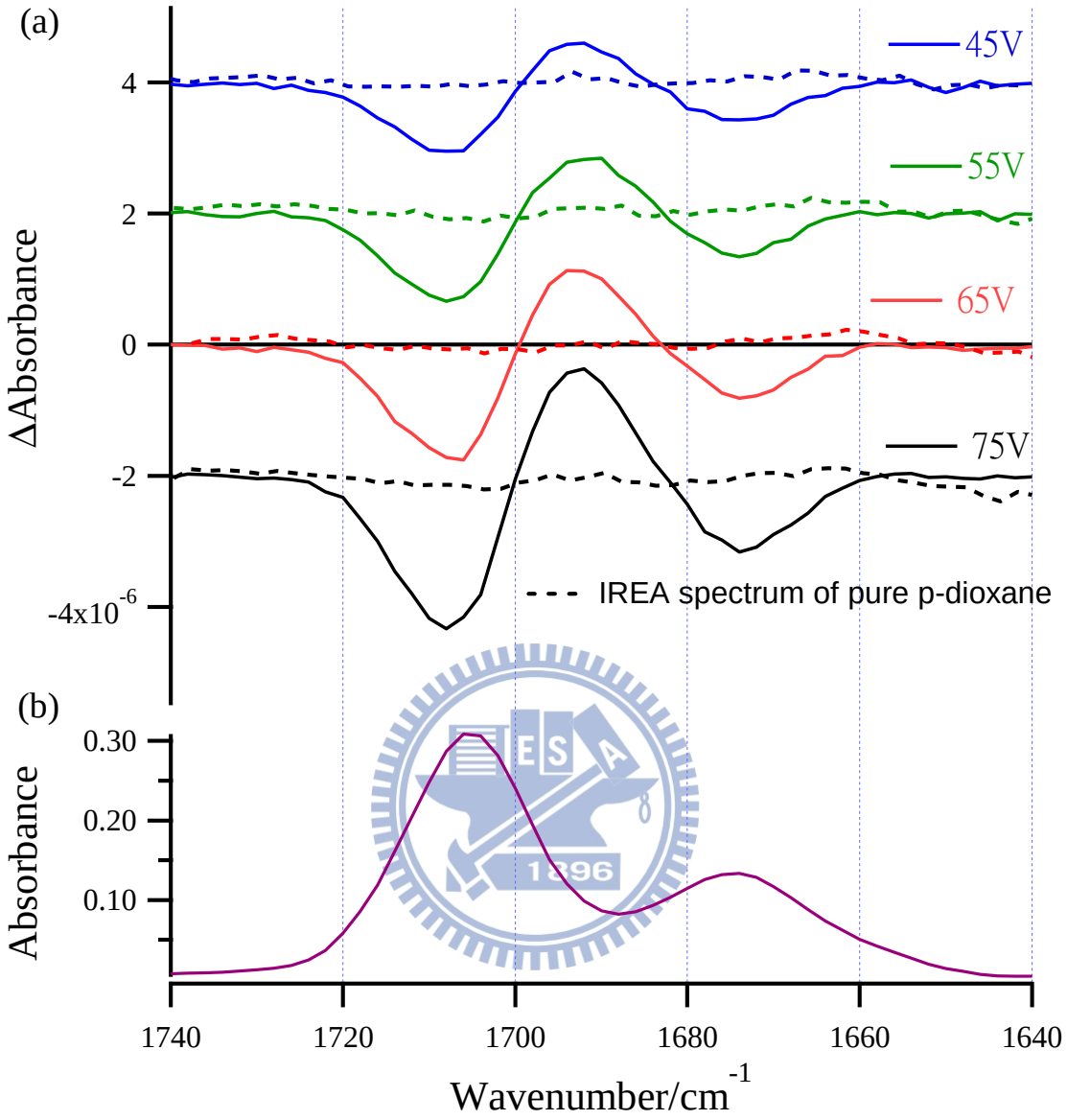

Figure IV-3. (a) Δ*A* spectra of 4(3H)-Pyr in *p*-dioxane (60 mM) measured with an applied voltage of 45, 55, 65, and 75V. (b) Absorption spectrum of 4(3H)-Pyr measured with a 50 μm path-length cell consisting CaF_2 windows.

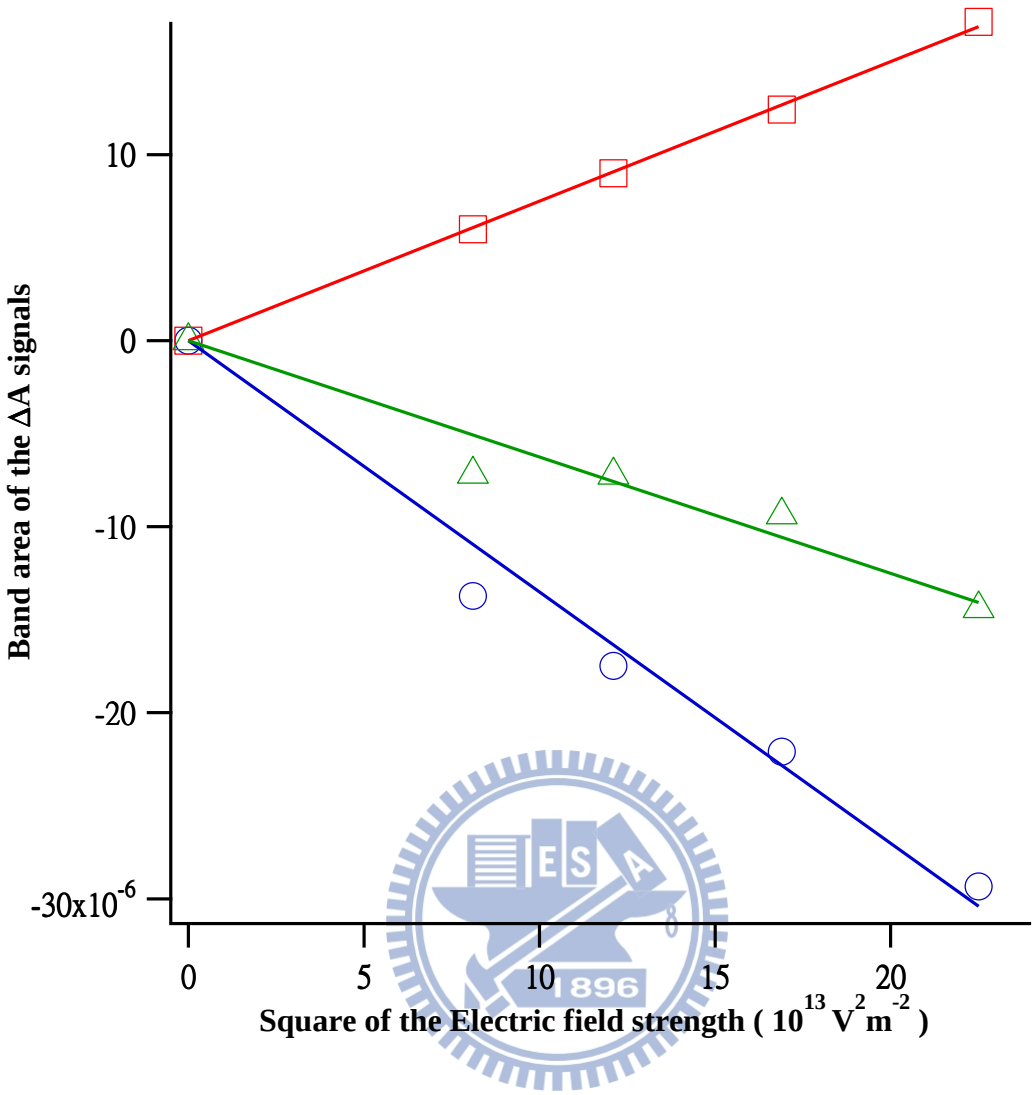

Figure IV-4. Band area of the Δ*A* signals for the 1722−1700 (blue circles), 1700−1682 (red squares), and 1682−1658 cm^{-1} (green triangles) region as a function of the square of external electric field. Solid lines are a fit to a linear function having a zero intercept.

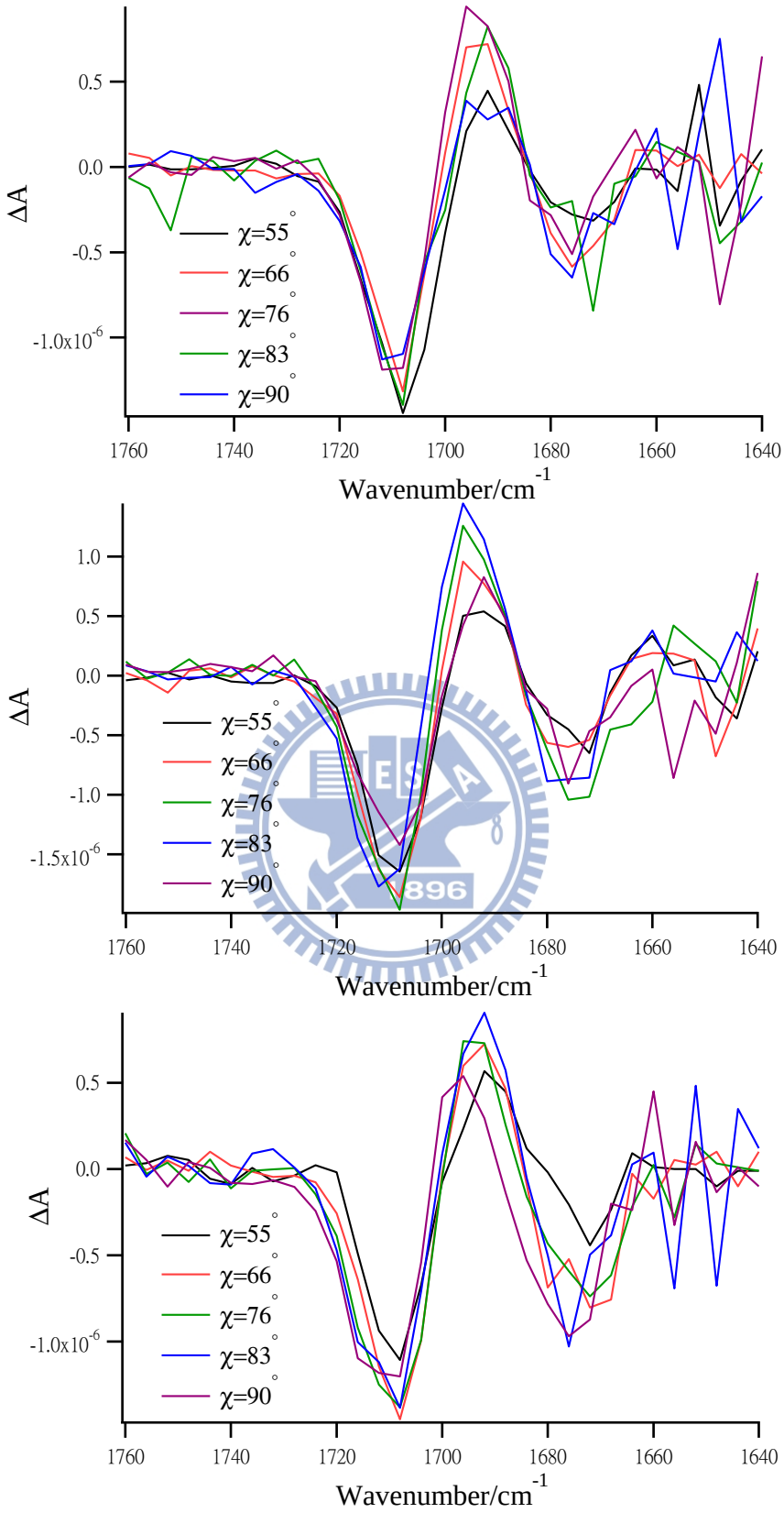

Figure IV-5. Three independent sets of the Δ*A* spectra of 4(3H)-Pyr in *p*-dioxane (60 mM) measured at χ = 55, 66, 76, 83, and 90°.

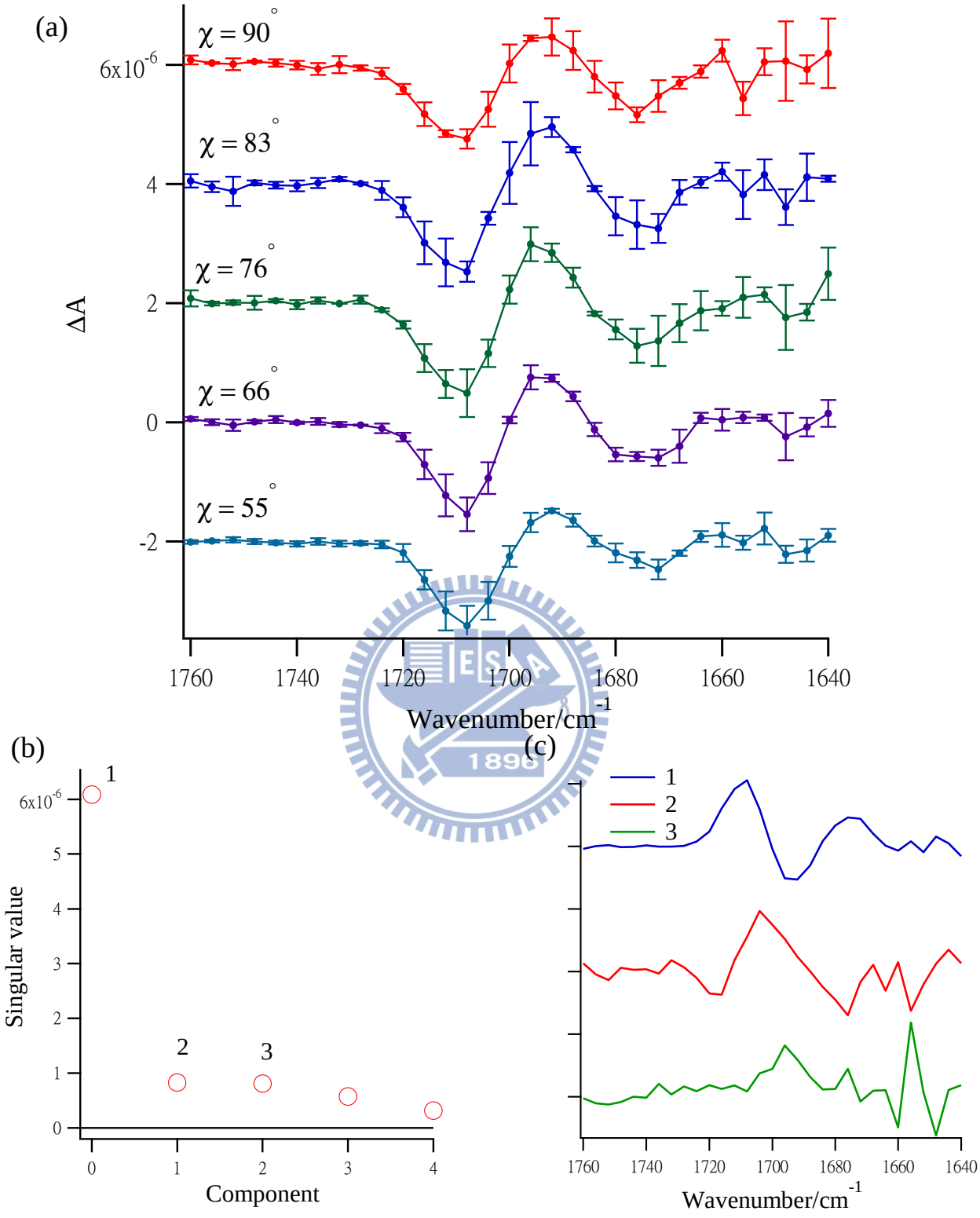

Figure IV-6. (a) Averaged χ-dependent ΔA spectra. (b) Plot of singular values obtained from the SVD of the averaged χ-dependent ΔA spectra shown in panel a. The components associated with the three largest singular values are denoted 1, 2, and 3. (c) Spectral components corresponding to the largest three singular values.

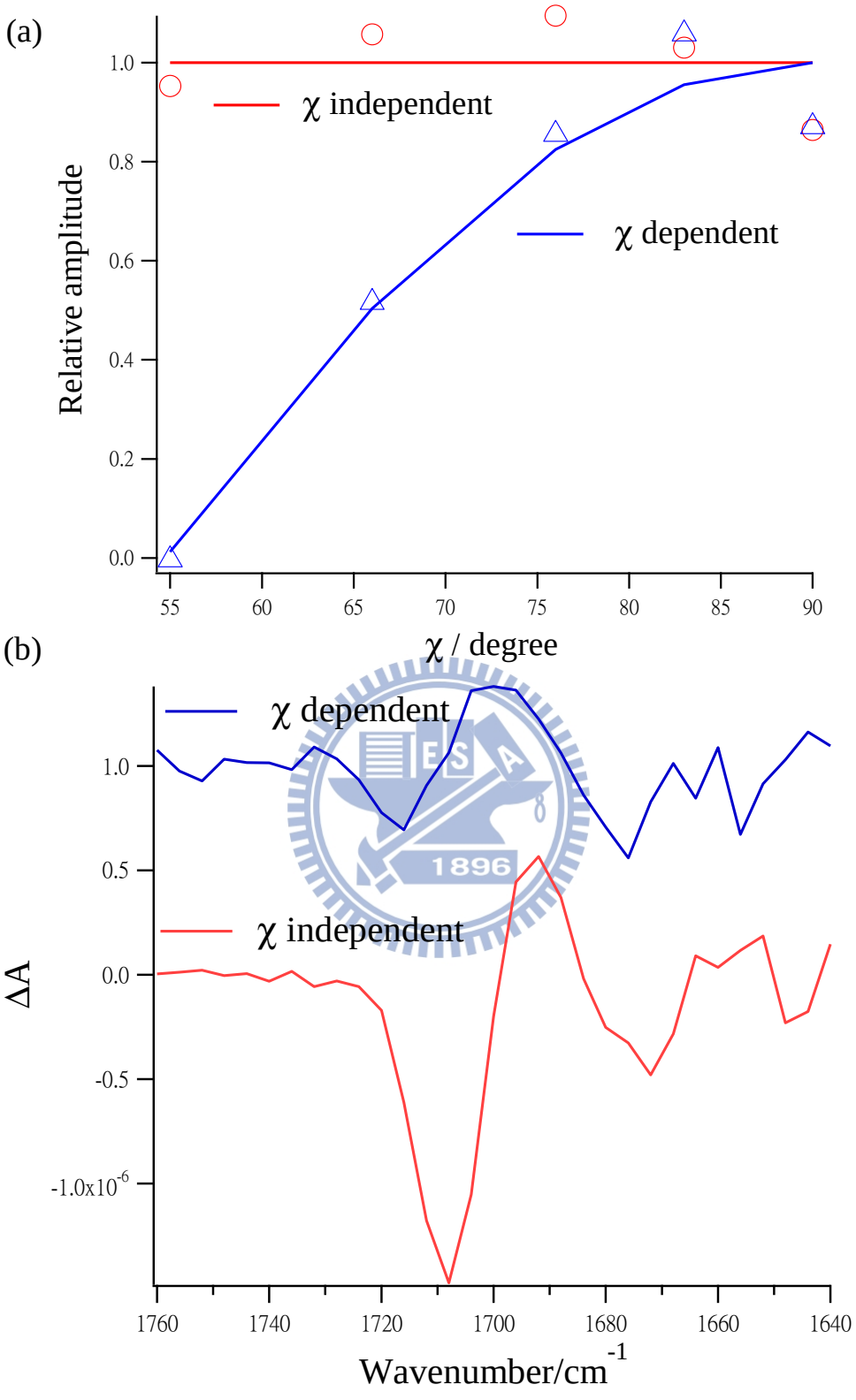

Figure IV-7. (a) Model functions (solid line) and reconstructed χ dependences (open triangles and circles). (b) χ-dependent (blue) and χ-independent (red) spectral components.

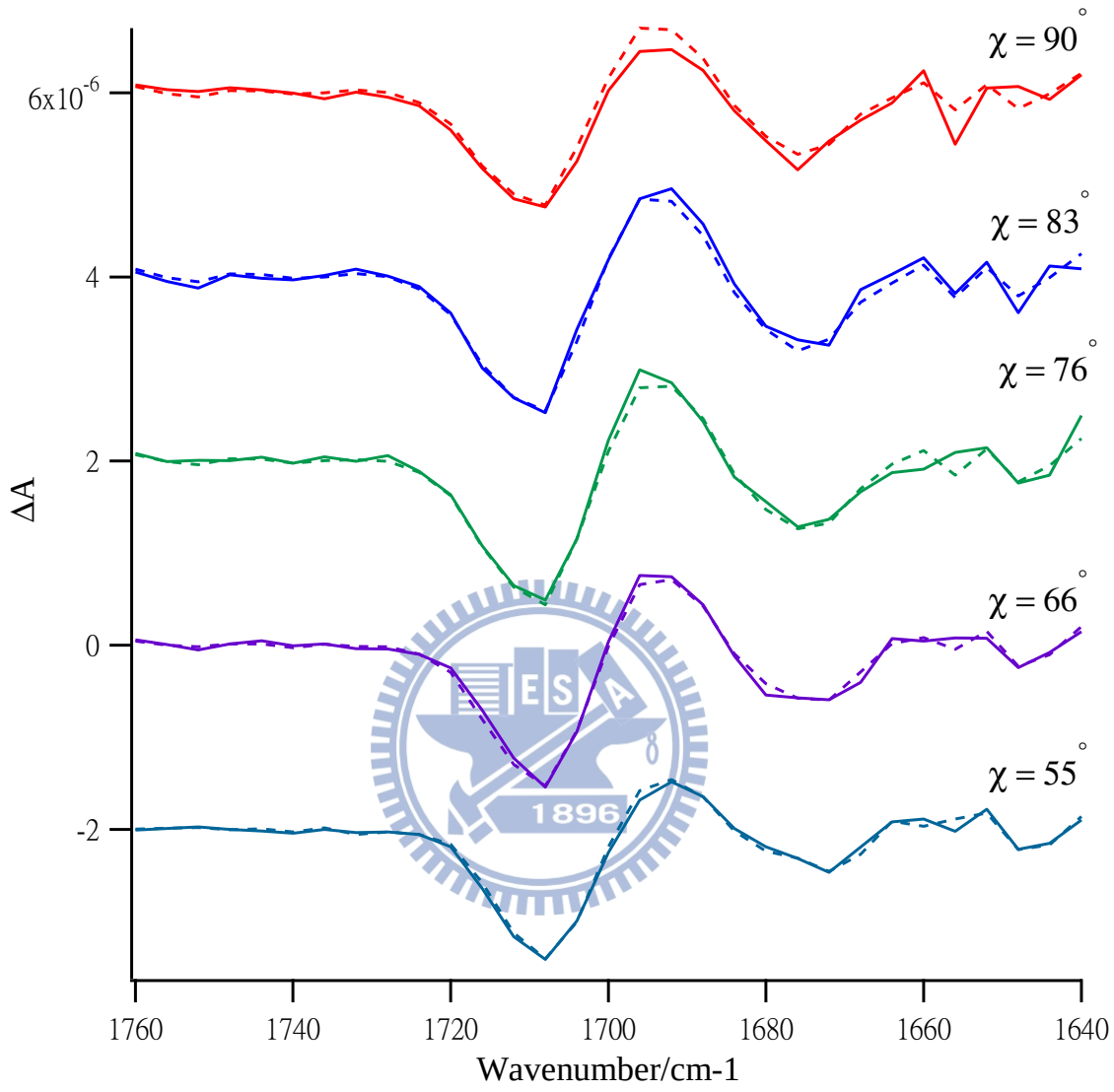

Figure IV-8. Observed (solid line) and reconstructed (dotted line) Δ*A* spectra of 4(3H)-Pyr in *p*-dioxane measured at χ = 55, 66, 76, 83, and 90°.

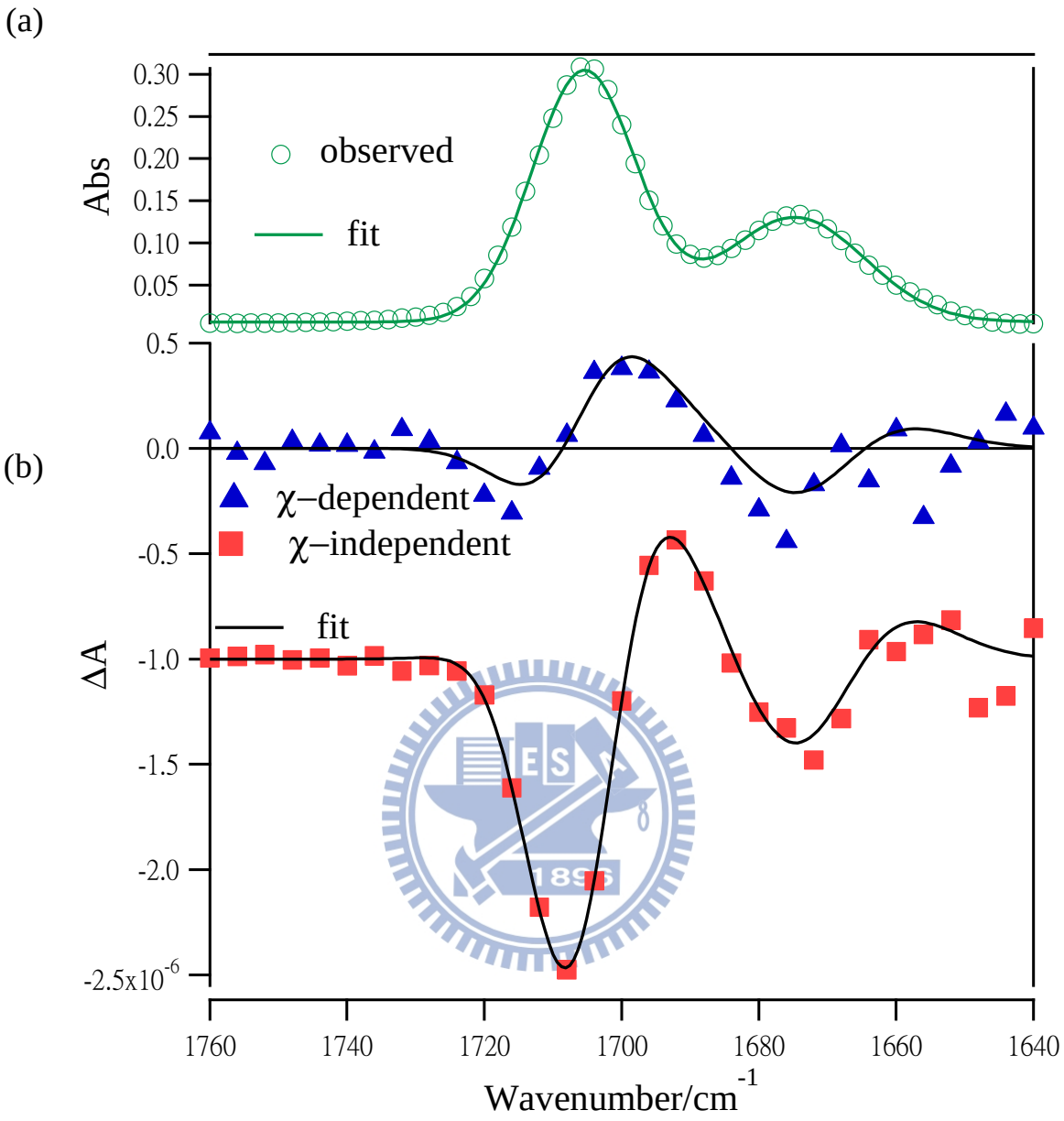

Figure IV-9. (a) IR absorption spectrum, the same as in Fig. IV-2(b). Also shown is the best fit to a sum of two Gaussian functions representing the C=O stretch bands of the monomer and the dimer of 4(3H)-Pyr. (b) χ-dependent (triangles) and χ-independent (squares) spectral components, and the best fit (solid curve) to a superposition of the zeroth, first, and second derivatives of the absorption bands.

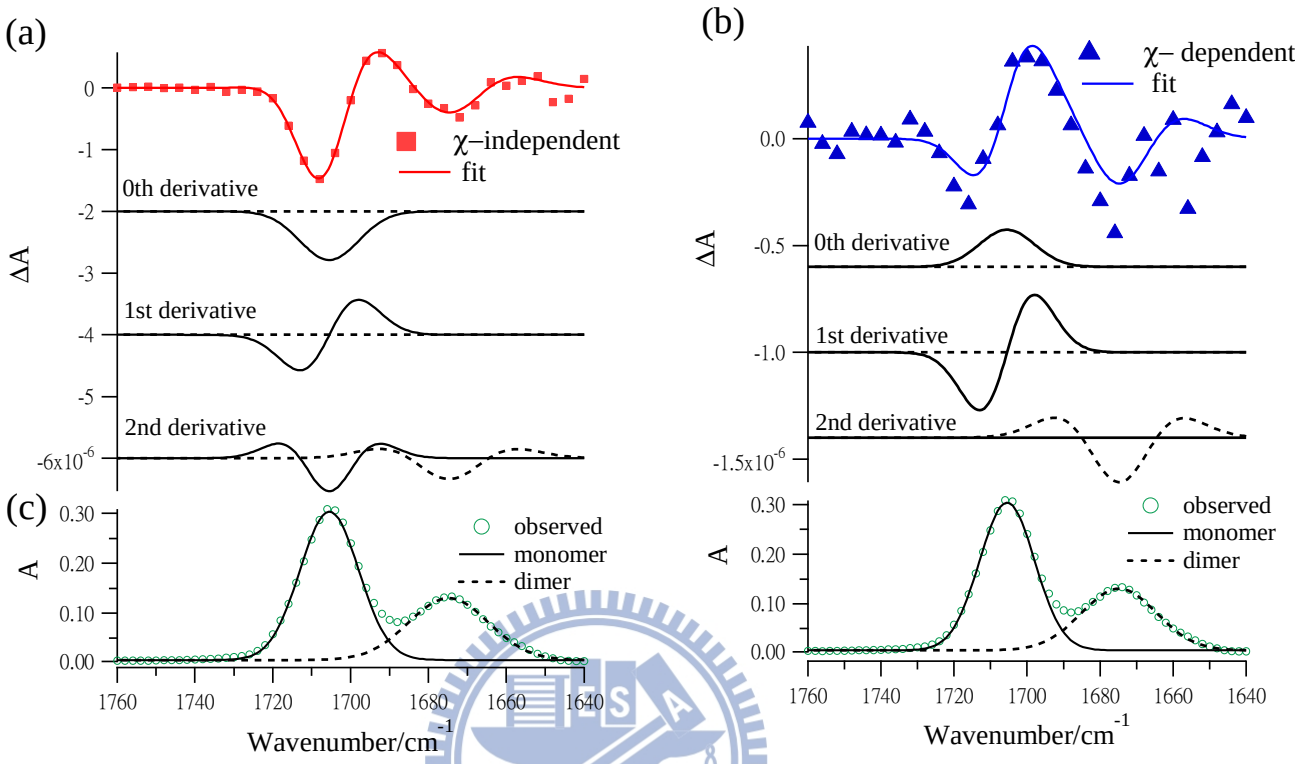

Figure IV-10. Decomposition of the fitted results in Fig. IV-8 into the zeroth, first, and second derivative components: (a) χ-independent and (b) χ-independent components. (c) Fitted result of the absorption spectrum.

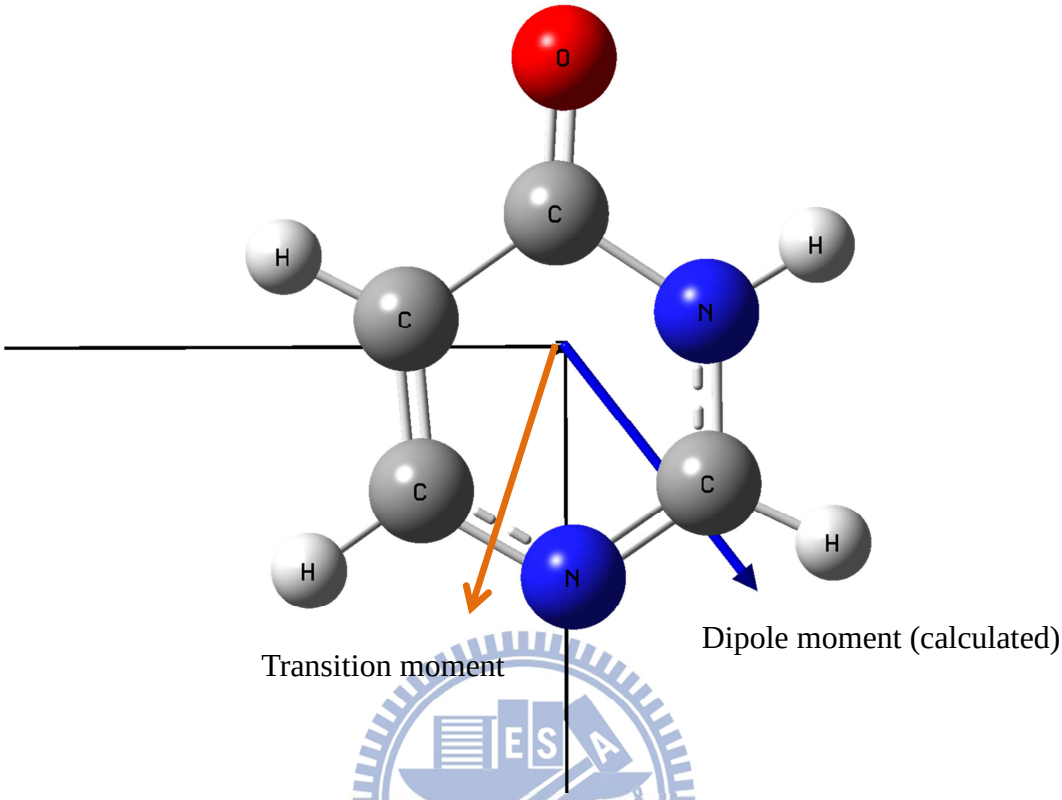

Figure IV-11. Predicted direction of the transition moment from the experimental results and the optimized structure of 4(3H)-Pyr calculated at the RB3LYP/6-31+G(d,p) level.

Table I. Assignments, peak positions, and bandwidths of the two IR bands observed in the wavenumber region 1740−1640 cm^{-1}.

Assignments	Peak position (cm^{-1})	Bandwidth (cm^{-1})
C=O stretch of the monomer of 4(3H)-Pyr	1706	11
C=O stretch of the dimer of 4(3H)-Pyr	1675	15

Table II. Coefficients a_χ, b_χ, and c_χ, of the zeroth, first, and second derivative terms of the absorption bands of 4(3H)-Pyr and its dimer. Note that $a_\chi = \Delta A/A$ and the absorbance A was taken from the spectrum measured with the 50-μm sample cell.

	χ-independent		χ-dependent	
	Monomer	Dimer	Monomer	Dimer
$a_\chi(10^{-6})$	−2.74	0[a]	0.58	0[a]
$b_\chi(10^{-5})$	2.32	0[a]	1.10	0[a]
$c_\chi(10^{-4})$	0.97	3.4	0[a]	1.78

[a] In the spirit of reducing the number of adjustable parameters, we set those coefficients zero.

Table III. Stark parameters A_χ, B_χ, and C_χ. Note that f is the local field correction factor.

	χ-independent		χ-dependent	
	Monomer	Dimer	Monomer	Dimer
$A_\chi(10^{-20}m^2V^{-2}f^{-2})$	−1.75	0[a]	0.37	0[a]
$B_\chi(10^{-43}Jm^2V^{-2}f^{-2})$	4.42	0[a]	2.10	0[a]
$C_\chi(10^{-66}J^2m^2V^{-2}f^{-2})$	0.73	2.58	0[a]	1.35

References

1. Bublitz, G.U. and S.G. Boxer, *Annual Review of Physical Chemistry*, 1997. **48**: p. 213.
2. Liptay, W., *Angewandte Chemie International Edition in English*, 1969. **8**: p. 177.
3. Ohta, N., *Bulletin of the Chemical Society of Japan*, 2002. **75**: p. 1637.
4. Liptay, W. *Excited states*. Vol.1, ed. E.C. Lim. 1974. 129.
5. Silverman, L.N., D.B. Spry, S.G. Boxer, and M.D. Fayer, *Journal of Physical Chemistry A*, 2008. **112**: p. 10244.
6. Mehata, M.S., K. Awasthi, T. Iimori, and N. Ohta, *Journal of Photochemistry and Photobiology A: Chemistry*, 2009. **204**: p. 39.
7. Mehata, M.S., C.-S. Hsu, Y.-P. Lee, and N. Ohta, *Journal of Physical Chemistry B*, 2010. **114**: p. 10234.
8. Yoshizawa, T., Y. Iwaki, N. Osaka, T. Nakabayashi, K.A. Zachariasse, and N. Ohta, *Journal of Physical Chemistry B*, 2004. **108**: p. 19132.
9. Handler, P. and D.E. Aspnes, *The Journal of Chemical Physics*, 1967. **47**: p. 473.
10. Chattopadhyay, A. and S.G. Boxer, *Journal of the American Chemical Society*, 1995. **117**: p. 1449.
11. Eun Sun, P. and S.G. Boxer, *Journal of Physical Chemistry B*, 2002. **106**: p. 5800.
12. Boxer, S.G., *Journal of Physical Chemistry B*, 2009. **113**: p. 2972.
13. Andrews, S.S. and S.G. Boxer, *Review of Scientific Instruments*, 2000. **71**: p. 3567.
14. Hiramatsu, H., C. Kato, and H. Hamaguchi, *Chemical Physics Letters*, 2001. **347**: p. 403.
15. Hiramatsu, H. and H. Hamaguchi, *Chemical Physics Letters*, 2002. **361**: p. 457.
16. Min, Y.K., H. Hiramatsu, and H. Hamaguchi, *Chemistry Letters*, 2002: p. 68.
17. Shigeto, S., H. Hiramatsu, and H. Hamaguchi, *Journal of Physical Chemistry A*, 2006. **110**: p. 3738.
18. Lee, I.C., H.-o. Hamaguchi, and S. Shigeto, *Chemical Physics Letters*, 2008. **466**: p.

144.

19. Wang, W.-C. and S. Shigeto, *Journal of Physical Chemistry A*, 2011. ***115***: p. 4448.

20. Nishida, J., S. Shigeto, S. Yabumoto, and H.-o. Hamaguchi, *The Journal of Chemical Physics*, 2012. **137**: p. 234501.

21. Yuzawa, T., C. Kato, M.W. George, and H.-O. Hamaguchi, *Appl. Spectrosc.*, 1994. **48**: p. 684.

22. Iwata, K. and H.-O. Hamaguchi, *Appl. Spectrosc.*, 1990. **44**: p. 1431.

23. Yabumoto, S., S. Shigeto, Y.-P. Lee, and H.-o. Hamaguchi, *Angewandte Chemie International Edition*, 2010. **49**: p. 9201.

24. Hiramatsu, H. and H. Hamaguchi, *Applied Spectroscopy*, 2004. **58**: p. 355.

25. Nakabayashi, T. and N. Ohta, *Chemistry Letters*, 2005. **34**: p. 1194.

26. Fafarman, A.T., L.J. Webb, J.I. Chuang, and S.G. Boxer, *Journal of the American Chemical Society*, 2006. **128**: p. 13356.

27. Dong, F. and R.E. Miller, *Science*, 2002. **298**: p. 1227.

28. Jalviste, E. and N. Ohta, *Journal of Photochemistry and Photobiology C: Photochemistry Reviews*, 2007. **8**: p. 30.

29. Ponder, M. and R. Mathies, *The Journal of Physical Chemistry*, 1983. **87**: p. 5090.

30. Accion, F., J. Tortajada, and J. Morcillo, *Journal of Molecular Structure*, 1986. **143**: p. 349.

31. Choi, M.Y., F. Dong, and R.E. Miller, *Philosophical Transactions of the Royal Society A: Mathematical, Physical and Engineering Sciences*, 2005. **363**: p. 393.

32. Choi, M.Y. and R.E. Miller, *Journal of the American Chemical Society*, 2006. **128**: p. 7320.

33. Choi, M.Y. and R.E. Miller, *The Journal of Physical Chemistry A*, 2007. **111**: p. 2475.

34. Dkhissi, A., L. Houben, J. Smets, L. Adamowicz, and G. Maes, *The Journal of Physical Chemistry A*, 2000. **104**: p. 9785.

35. Lapinski, L., J. Fulara, and M.J. Nowak, *Spectrochimica Acta Part a-Molecular and Biomolecular Spectroscopy*, 1990. **46**: p. 61.

36. Lapinski, L., M.J. Nowak, A. Les, and L. Adamowicz, *Vibrational Spectroscopy*, 1995. **8**: p. 331.

37. Mons, M., I. Dimicoli, F. Piuzzi, B. Tardivel, and M. Elhanine, *The Journal of Physical Chemistry A*, 2002. **106**: p. 5088.

38. Nir, E., C. Janzen, P. Imhof, K. Kleinermanns, and M.S. de Vries, *Physical Chemistry Chemical Physics*, 2002. **4**: p. 740.

39. Nosenko, Y., M. Kunitski, T. Stark, M. Göbel, P. Tarakeshwar, and B. Brutschy, *Physical chemistry chemical physics : PCCP*, 2013. **15**: p. 11520.

40. Padermshoke, A., Y. Katsumoto, and M. Aida, *The Journal of Physical Chemistry B*, 2006. **110**: p. 26388.

41. Szczesniak, M., M.J. Nowak, H. Rostkowska, K. Szczepaniak, W.B. Person, and D. Shugar, *Journal of the American Chemical Society*, 1983. **105**: p. 5969.

42. Zwier, T.S., *The Journal of Physical Chemistry A*, 2001. **105**: p. 8827.

43. Choi, M.Y. and R.E. Miller, *The Journal of Physical Chemistry A*, 2006. **110**: p. 9344.

44. Watson, J.D. and F.H.C. Crick, *Nature*, 1953. **171**: p. 964.

45. Kim, H. and M. Cho, *Chemical Reviews*, 2013.

46. Nowak, M.J., K. Szczepaniak, A. Barski, and D. Shugar, *Journal of Molecular Structure*, 1980. **62**: p. 47.

47. Nowak, M.J., J. Fulara, and L. Lapinski, *Journal of Molecular Structure*, 1988. **175**: p. 91.

48. Schneider, W.C., *Journal of the American Chemical Society*, 1948. **70**: p. 627.

49. Tanaka, S., C. Kato, K. Horie, and H.-o. Hamaguchi, *Chemical Physics Letters*, 2003. **381**: p. 385.

50. Mohanalingam, K., D. Yokoyama, C. Kato, and H.-o. Hamaguchi, *Bulletin of the*

Chemical Society of Japan, 1999. **72**: p. 389.

51. Radziszewski, J.G., V. Balaji, P. Carsky, and E.W. Thulstrup, *The Journal of Physical Chemistry*, 1991. **95**: p. 5064.

52. Radziszewski, J.G., J.W. Downing, M.S. Gudipati, V. Balaji, E.W. Thulstrup, and J. Michl, *Journal of the American Chemical Society*, 1996. **118**: p. 10275.